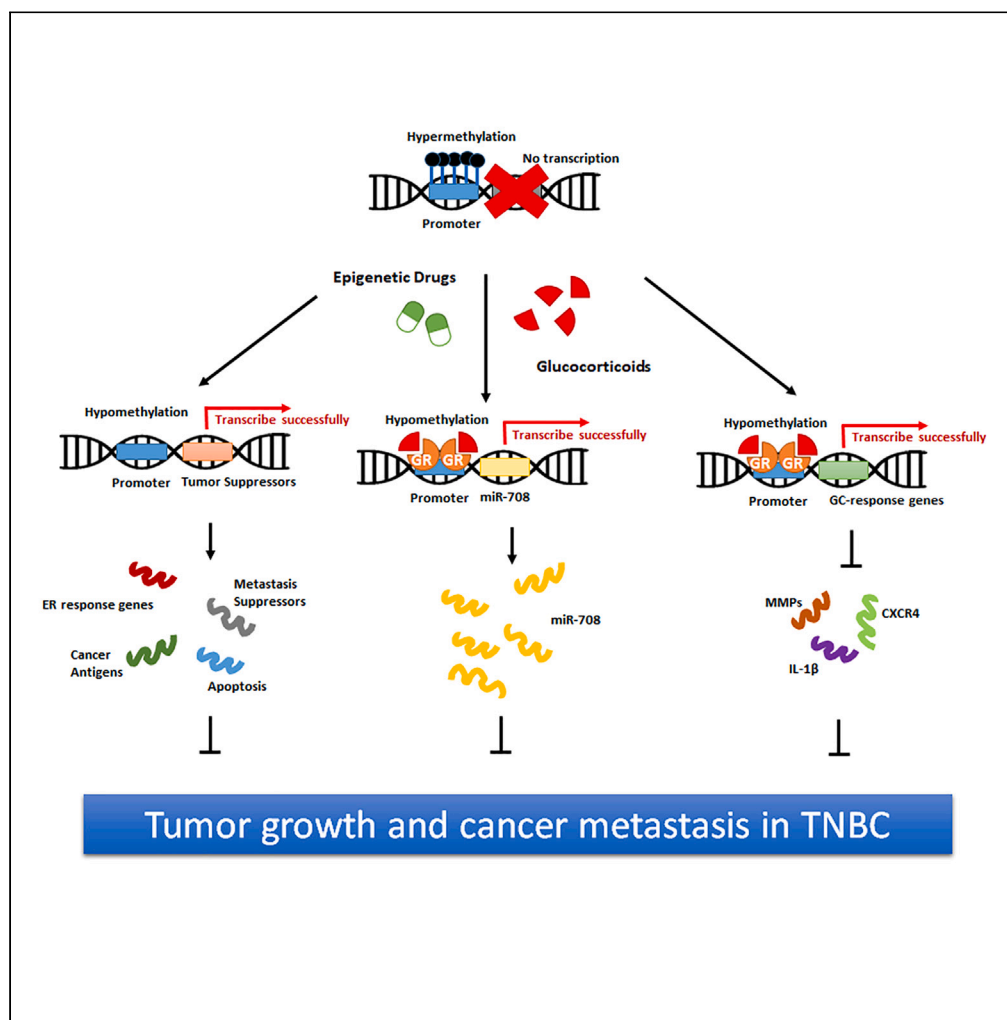


Article

Combating breast cancer progression through combination therapy with hypomethylating agent and glucocorticoid



Yu-Hsin Chu, Yi-Chen Huang, Pei-Yun Chiu, ..., Yi-Hsiang Wang, Yi-Fan Lin, Kai-Ti Lin

ktlin@life.nthu.edu.tw

Highlights

The miR-708 promoter region is methylated and correlated with a poor prognosis

The expression of microRNA-708 correlates with better clinical in TNBC patients

The combination of decitabine and glucocorticoid can suppress TNBC progression

Cotreatment with glucocorticoid reduces decitabine-stimulated MMPs and IL-1



Article

Combating breast cancer progression through combination therapy with hypomethylating agent and glucocorticoid

Yu-Hsin Chu,^{1,5} Yi-Chen Huang,^{1,5} Pei-Yun Chiu,^{1,5} Wen-Hung Kuo,² Yan-Ru Pan,¹ Yuan-Ting Kuo,¹ Rong-Hsuan Wang,¹ Yu-Chin Kao,¹ Yi-Hsiang Wang,⁴ Yi-Fan Lin,¹ and Kai-Ti Lin^{1,3,6,*}

SUMMARY

Breast cancer is the leading cause of cancer-related death in women. Among breast cancer types, triple-negative breast cancer (TNBC) accounts for 15% of all breast cancers with aggressive tumor behavior. By using bioinformatic approaches, we observed that the microRNA-708 promoter is highly methylated in breast carcinomas, and this methylation is linked to a poor prognosis. Moreover, microRNA-708 expression correlates with better clinical outcomes in TNBC patients. Combination treatment with the hypomethylating agent decitabine and synthetic glucocorticoid significantly increased the expression of microRNA-708, reactivated DNMT-suppressed pathways, and decreased the expression of multiple metastasis-promoting genes such as matrix metalloproteinases (MMPs) and IL-1 β , leading to the suppression of breast cancer cell proliferation, migration, and invasion, as well as reduced tumor growth and distant metastasis in the TNBC xenograft mouse model. Overall, our study reveals a therapeutic opportunity in which a combined regimen of decitabine with glucocorticoid may have therapeutic potential in treating TNBC patients.

INTRODUCTION

Breast cancer is heterogeneous cancer that consists of many different cell types.¹ Based on histological analyses of the levels of estrogen receptor (ER), progesterone receptor (PR), and human epidermal growth factor receptor 2 (HER2), breast cancer can be subdivided into luminal A, luminal B, HER2-enriched, and basal-like types. The majority of basal-like breast cancers lack ER, PR, and HER2 expression; thus, this type of tumor is also called triple-negative breast cancer (TNBC). Despite advances in the recently developed treatment options to target HER2 or hormone receptors, targeted therapies are still unavailable for TNBC, and only approximately 50% of patients respond to standard chemotherapy.² Studies unveiling the molecular mechanism of TNBC progression are urgently needed to develop new strategies for treating patients with this tumor subtype.

Breast cancer initiation and progression are due to the accumulation of pathological alterations in gene expression, such as oncogene overexpression and tumor suppressor loss.³ In contrast to genetic mutations, acquired epigenetic abnormalities have been observed in many cancer types, including DNA methylation, histone modifications, and nucleosome remodeling.⁴ In breast cancer, emerging evidence indicates that epigenetic reprogramming is a common feature that sustains tumorigenesis and metastasis.⁵ Accordingly, targeting epigenetic abnormalities in cancer cells is considered an effective strategy in breast cancer therapy.⁶ Many compounds have been developed to control epigenetic modification, including DNA methylation, histone methylation, and histone acetylation. Decitabine (DAC), a DNA methyltransferase (DNMT) inhibitor, is an FDA-approved hypomethylating drug⁷ to treat patients with myelodysplastic syndrome⁸ and acute myeloid leukemia.⁹ In breast cancer, DAC as monotherapy only results in moderate response rates (35%).¹⁰ Combination therapy with other chemotherapy or immunotherapy is currently evaluated in multiple clinical trials to enhance anti-tumor efficacy.^{11,12} A study on patient-derived xenograft (PDX) organoids showed the promising therapeutic potential of using DAC to treat TNBC,¹³ and the use of DAC in combination with other drugs to treat patients with TNBC is currently under investigation in multiple clinical trials, including NCT02957968 and NCT03295552.

¹Institute of Biotechnology, College of Life Science, National Tsing Hua University, Hsinchu, Taiwan

²Department of Surgery, National Taiwan University Hospital, Taipei, Taiwan

³Department of Medical Science, College of Life Science, National Tsing Hua University, Hsinchu, Taiwan

⁴Institute of Molecular Medicine, College of Life Science, National Tsing Hua University, Hsinchu, Taiwan

⁵These authors contributed equally

⁶Lead contact

*Correspondence: ktlin@life.nthu.edu.tw

<https://doi.org/10.1016/j.isci.2023.106597>



MicroRNAs (miRNAs) are small noncoding RNAs that function in the regulation of gene expression. Dysregulation of miRNAs has been shown to promote cancer progression in human tumors.^{14,15} Among these miRNAs, miR-708 is downregulated and functions as a tumor suppressor in many cancer types.^{16–22} Correlated with reduced expression, epigenetic changes were observed in the promoter regions of miR-708, including DNA hypermethylation^{23–25} and histone trimethylation,^{16,25,26} indicating that miR-708 expression is suppressed through epigenetic modifications in cancer cells to facilitate cancer progression. In breast cancer, the expression of miR-708 is substantially suppressed in metastatic breast cancer cells and metastatic lymph nodes collected from breast cancer patients.¹⁶ By targeting Rap1B,²⁷ CD44,²⁸ Ikk β ,²⁸ neurotatin,¹⁶ LSD1,²⁹ and B7-H3,³⁰ miR-708 inhibits breast cancer progression by repressing migration, invasion, proliferation, and potentially immune modulation. Nanoparticle-mediated delivery of miR-708 successfully impaired TNBC metastasis in a mouse model *in vivo*,³¹ revealing that miR-708 is a suitable therapeutic target in treating breast cancer metastasis.

Glucocorticoid (GC) is known to exert pronounced effects on metabolism, differentiation, proliferation, and survival.³² In breast cancer, synthetic GC is widely used as a comedication with chemotherapy to reduce adverse effects caused by chemotherapy.³³ Although recent studies have reported controversial results that a high dose of GC in GR-activated cells promotes metastasis in the xenograft mouse model,³⁴ no significant difference in breast cancer recurrence was observed compared to patients with breast cancer who received chemotherapy concurrently with GC and those who did not.³⁵ In contrast, comedication with GC even improved survival in breast cancer patients receiving adjuvant anthracycline-based chemotherapy.³⁶ Our previous study showed an interesting phenomenon in which synthetic GC inhibits breast cancer tumor growth and metastasis at the low dose, whereas GC at the high dose promotes breast cancer progression,²⁷ reflecting the safety and potential application of using low-dose GC to suppress breast cancer progression.

Studies on miR-708 have highlighted its emerging roles in multiple pathways to suppress cancer progression,³⁷ revealing the potential use of miR-708 as a therapeutic target. Here, we characterized that the combined regimen of DNA-demethylating agent DAC, together with low-dose synthetic GC, dexamethasone (DEX), work significantly to suppress TNBC tumor growth and distant metastasis through three independent pathways, including reactivation of DNMT-suppressed pathways, induction of miR-708 expression, and suppression of NF- κ B-induced metastasis promoting genes. In summary, our study reveals that the combination strategy of DAC and DEX may provide a novel therapeutic window for TNBC, a currently incurable disease.

RESULTS

The expression of miR-708 is suppressed in metastatic lymph nodes and negatively correlates with survival in patients with TNBC

We analyzed miR-708 expression in clinical breast cancer carcinomas (T), adjacent nontumor tissue (N), and metastatic lymph nodes (LN), from National Taiwan University Hospital (NTUH) using real-time RT-qPCR to evaluate the clinical relevance of miR-708 in breast cancer progression. The expression of miR-708 was significantly decreased in metastatic lymph nodes (LN) and primary tumors (T) compared to adjacent nontumor tissues (N; Figure 1A). Previous studies showed the significant suppression of miR-708 expression in TNBC cell lines.^{16,27} We further subdivided clinical samples into TNBC and non-TNBC groups to investigate whether the expression of miR-708 is suppressed in tumors isolated from patients with TNBC. Consistent with previous observations, the expression of miR-708 was substantially suppressed in both primary tumors and metastatic lymph nodes from the TNBC group compared to the non-TNBC group (Figure 1B). We also observed reduced expression of miR-708 in breast tumor samples compared to breast normal tissues from The Cancer Genome Atlas (TCGA) public dataset (Figure S1A). A detailed analysis revealed that the expression of miR-708 remained similar when we compared samples based on cancer staging, grading, metastasis, and TNBC or non-TNBC (Figures S1A–S1D). The survival curve comparing the patients with high (red) or low (black) expressions was plotted using the Kaplan-Meier Plotter database to further explore the clinical significance of miR-708 in breast cancer. A total of 1,262 and 1,061 breast cancer specimens were included from the METABRIC and TCGA databases, respectively. The expression of miR-708 was not strongly correlated with the overall survival of patients with all subtypes of breast cancer (Figure 1C). Instead, high miR-708 expression resulted in prolonged overall survival only in patients with TNBC (Figure 1D), revealing the therapeutic potential of miR-708 in treating patients with TNBC. Overall, our data indicated that miR-708 expression was decreased and correlated with poor overall survival in TNBC patients.

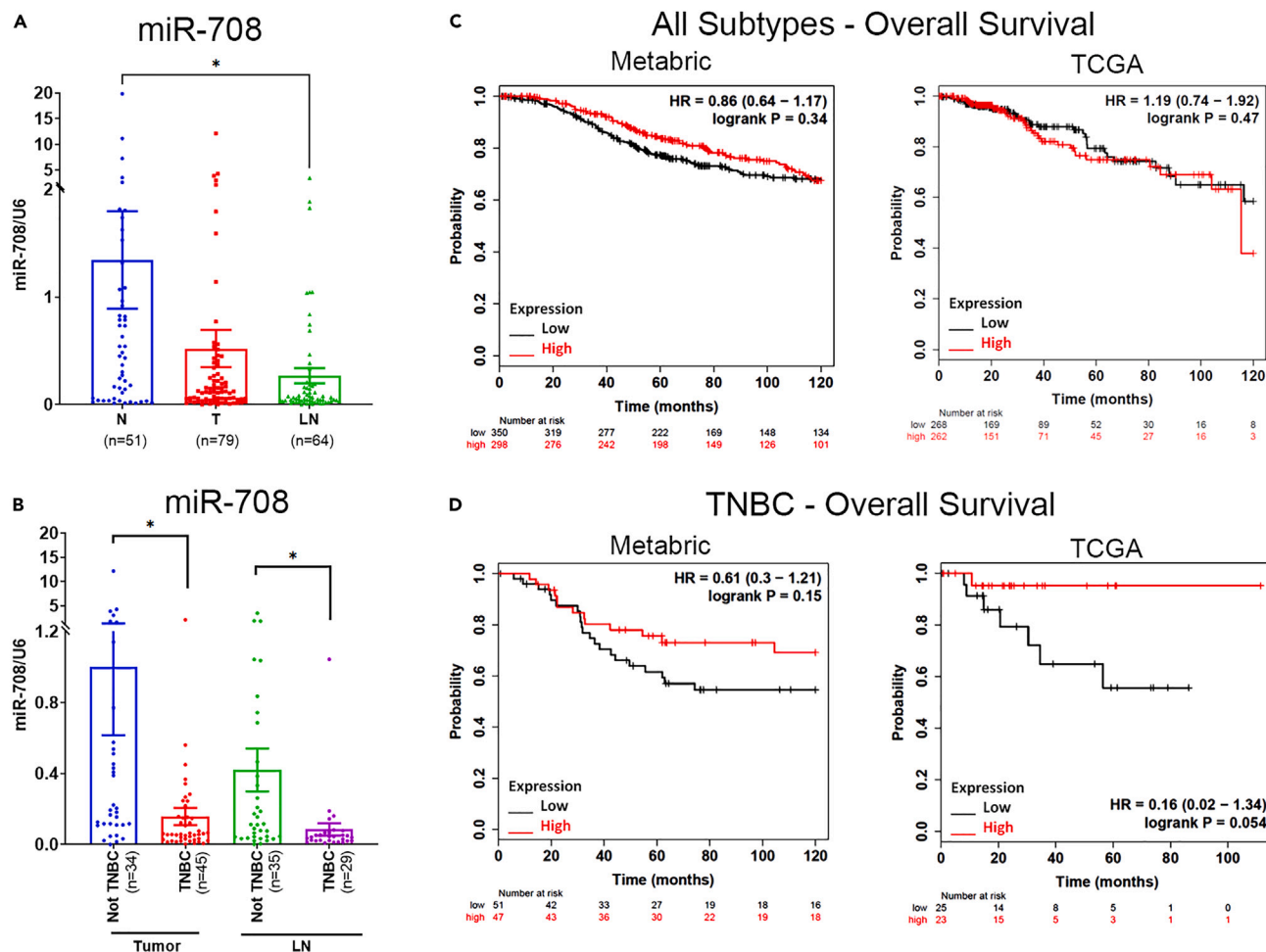


Figure 1. The expression of miR-708 is suppressed in breast tumor samples and correlates with poor survival in patients with TNBC

(A) Expression of miR-708 in adjacent nontumor (N), primary tumor (T), and lymph node metastasis (LN). Clinical samples were obtained from NTUH. Data are presented as means \pm SEM. ANOVA followed by Tukey's post hoc test was used for the statistical analysis (* $p < 0.05$).

(B) Clinical data from (A) of primary tumors (T) and lymph node metastases (LN) were further subdivided into TNBC and non-TNBC groups. Data are presented as means \pm SEM. Student's t test was used for the statistical analysis (* $p < 0.05$).

(C) Kaplan-Meier overall survival analysis of patients with all subtypes of breast cancer presenting high or low (Q1 versus Q4) miR-708 expression. The miRNA array data for miR-708 were obtained from the METABRIC cohorts ($n = 1262$) and TCGA cohorts ($n = 1061$). The p value was calculated using the log rank test.

(D) Kaplan-Meier overall survival analysis of patients with TNBC presenting high or low (Q1 versus Q4) miR-708 expression. The miRNA array data for miR-708 were obtained from the METABRIC cohorts ($n = 203$) and TCGA cohorts ($n = 97$). The p value was calculated using the log rank test.

MicroRNA-708 is epigenetically silenced in breast cancer

Aberrant DNA hypermethylation of CpG islands in the promoter regions of tumor suppressors is an important mechanism by which gene silencing promotes cancer progression.³⁸ Consistent with many other tumor suppressors, studies have shown that the promoter of miR-708 is hypermethylated in chronic lymphocytic leukemia (CLL)^{23,24} and glioma.²⁵ Since miR-708 expression was markedly suppressed in clinical samples of breast tumors (Figure 1A), we next tried to determine whether the promoter region of miR-708 is epigenetically suppressed in breast cancer cells. As shown in the previous study, the putative promoter region of miR-708 is inside the CpG islands in the first intron of the host gene ODZ4.¹⁷ We analyzed and compared the DNA methylation status on this putative promoter region (Shown as R1 and R2 in Figure 2A) between MCF-10A and MDA-MB-231 cells using bisulfite sequencing to determine whether the promoter region of miR-708 is methylated in metastatic breast cancer cells. The promoter region of miR-708 was hypermethylated in both R1 and R2 regions in MDA-MB-231 cells, while those regions remained unmethylated in normal MCF-10A cells (Figures 2B and 2C), suggesting that the reduced miR-708 expression was due to hypermethylation of its promoter in metastatic breast cancer cells.

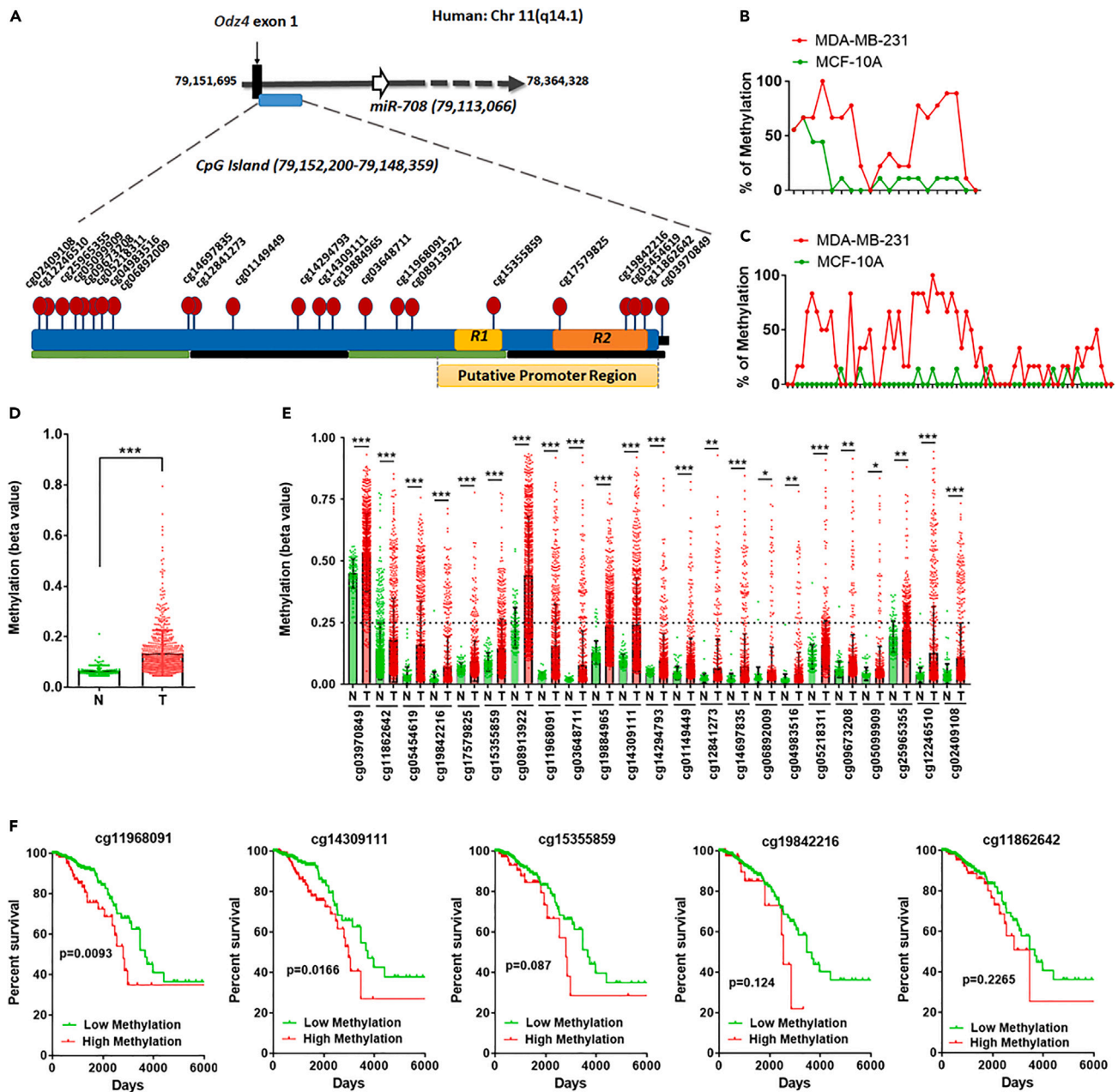


Figure 2. The promoter region of miR-708 is highly methylated in breast cancer, and higher methylation in this region correlates with shorter survival

(A) Schematic graph illustrating the genomic locations of miR-708 and its host gene, ODZ4. The CpG island and putative promoter region are indicated as blue and orange bars. The CpG island is further enlarged to illustrate the location of R1, R2, and CpG probes used in bisulfite sequencing and methylation array.

(B and C) Bisulfite analysis of the change in DNA methylation at R1 (B) and R2 (C) in the miR-708 promoter region between the normal breast epithelial cell line MCF-10A and the metastatic TNBC line MDA-MB-231. The percentage of methylation at each individual CpG site was calculated based on the bisulfite conversion result obtained from the ten clones.

(D and E) Promoter methylation levels of miR-708 in breast carcinomas (TCGA Wanderer web). Mean methylation levels among all CpG islands (D) and mean methylation levels of different CpG probes in the CpG islands of the miR-708 promoter (E). Data are presented as means \pm SD. Student's *t* test was used for the statistical analysis (**p* < 0.05; ***p* < 0.01; ****p* < 0.001).

(F) Kaplan-Meier survival analysis of samples from the breast carcinoma database of TCGA Wanderer web with high methylation (beta value >0.25) or low methylation (beta value \leq 0.25) levels at specific CpG probes, including cg11968091, cg14309111, cg15355859, cg19842216, and cg11862642. Statistical significance was determined using the χ^2 test. Detailed information for the locations of R1, R2, and CpG probes is provided in [Table S2](#).

We next tried to analyze the CpG islands presenting in the miR-708 promoter from the TCGA database using the online tool Wanderer to further characterize the methylation status of the miR-708 promoter in clinical samples.³⁹ The mean methylation levels among all CpG islands were significantly increased in the tumor samples compared to the adjacent nontumor samples (Figure 2D). Moreover, each individual CpG site in this area was highly methylated in the tumor samples (Figure 2E), suggesting that the highly suppressed miR-708 expression we observed in clinical tumor samples (Figure 1A and S1A) is mainly mediated by DNA methylation. We further compared the methylation levels at the miR-708 promoter region in patients with TNBC or non-TNBC and found no significant difference (Figures S2A and S2B), similar to the miR-708 expression profile we observed from the same TCGA cohort (Figure S1D). We then tried to determine whether the methylation level at each of these CpG sites correlated with the prognosis of patients with breast cancer. The Kaplan-Meier analysis showed that higher levels of DNA methylation at these CpG sites, especially at cg11968091 and cg14309111, correlated with shorter survival (Figure 2F), suggesting that the methylation level of this CpG island may serve as a potential prognostic marker for the survival of patients with breast cancer. Overall, we conclude that the promoter region of miR-708 is highly methylated in breast tumors as compared to adjacent normal tissues (Figures 2B–2E). Interestingly, based on the prognosis analysis we observed from breast cancer patients (Figures 1C and 1D), expression of miR-708 only showed survival benefits in TNBC patients. Since miR-708 acts as a metastatic suppressor microRNA^{16,17} and TNBC is the most aggressive breast cancer subtype with high metastatic potential,⁴⁰ we believe that miR-708, which correlates with better survival clinically, may serve as a perfect therapeutic target for TNBC patients.

The combined regimen of DEX and DAC significantly increases the expression of miR-708 in TNBC cells

Previous studies showed the significant suppression of miR-708 expression in multiple different TNBC cell lines, while higher miR-708 expression was observed in normal MCF-10A cells and ER-positive MCF-7 cells.^{16,27} To confirm whether the miR-708 expression is tightly regulated by epigenetic modifications in TNBC cell lines, we treated cells with the DNA demethylation drug, DAC. Interestingly, miR-708 expression did not change or even be suppressed upon treatment with DAC in normal MCF-10A cells (Figure 3A) or ER-positive MCF-7 cells (Figure S3A), respectively. In contrast, treatment with DAC alone resulted in a 10-fold increase in miR-708 expression in the metastatic TNBC cells, MDA-MB-231, (Figure 3B), confirming our hypothesis that miR-708 is epigenetically silenced in TNBC cells. Amazingly, cotreatment with DAC and DEX synergistically increased miR-708 expression by more than 100-fold compared to the control (Figure 3B). A similar synergistic induction of miR-708 expression by cotreatment with DAC and DEX was also observed in other TNBC cell lines, including HCC-1395 (Figure 3C) and Hs578T (Figure 3D), indicating that the combination of these two drugs effectively induced miR-708 expression in TNBC cells. We further examined whether the expression of the miR-708 downstream target, Rap1B,¹⁷ CD44,¹⁸ or IKK β ,²³ was affected by cotreatment with DAC and DEX. Interestingly, we found that both Rap1B and CD44 mRNAs were upregulated in cells treated with DAC alone, which may be caused by the DAC-mediated demethylation on the promoter region of Rap1B and CD44 to accelerate their transcriptions (Figure 3E). This induction was then reduced in cells cotreated with DAC and DEX in MDA-MB-231 (Figure 3E) and HCC-1395 cells (Figure S3B). In contrast, expression of IKK β mRNAs was upregulated in MDA-MB-231 cells treated with DAC alone or DAC+DEX, no reduction was observed in cells cotreated with DAC and DEX (Figure S3C). Since miR-708 may not only inhibit mRNA stability but also repress protein translation, we then checked protein levels. Interestingly, we found that, unlike mRNA level (Figures 3E and S3C), expression of Rap1B, CD44, or IKK β protein was not induced in DAC-treated cells. Inhibition of Rap1B and CD44 protein expression was observed in cells cotreated with DAC and DEX, as compared to the DAC or DEX treatment alone (Figure 3F), while the level of IKK β was reduced in cells treated with DEX alone or DEX plus DAC (Figure S3D). Since Rap1B is an important mediator of cell motility,¹⁷ CD44 is a tumor stemness marker,^{18,28} and IKK β is an NF- κ B activator to promote inflammation and tumorigenesis,⁴¹ the reduced protein expressions of these three genes by DAC and DEX may be useful to improve the disease outcome.

The combined regimen of DEX and DAC reactivates genes suppressed by DNMT-mediated pathways and impairs genes involved in ribosome biogenesis

We performed the RNA sequencing (RNA-seq) analysis to compare the difference in the transcriptional profile of MDA-MB-231 cells treated with the control, DEX, DAC, or DEX plus DAC and to further analyze the downstream signaling pathways affected by these two drugs (Figure S4A). Three biological replicates were included for each treatment, and gene expression patterns were distinct in different treatment

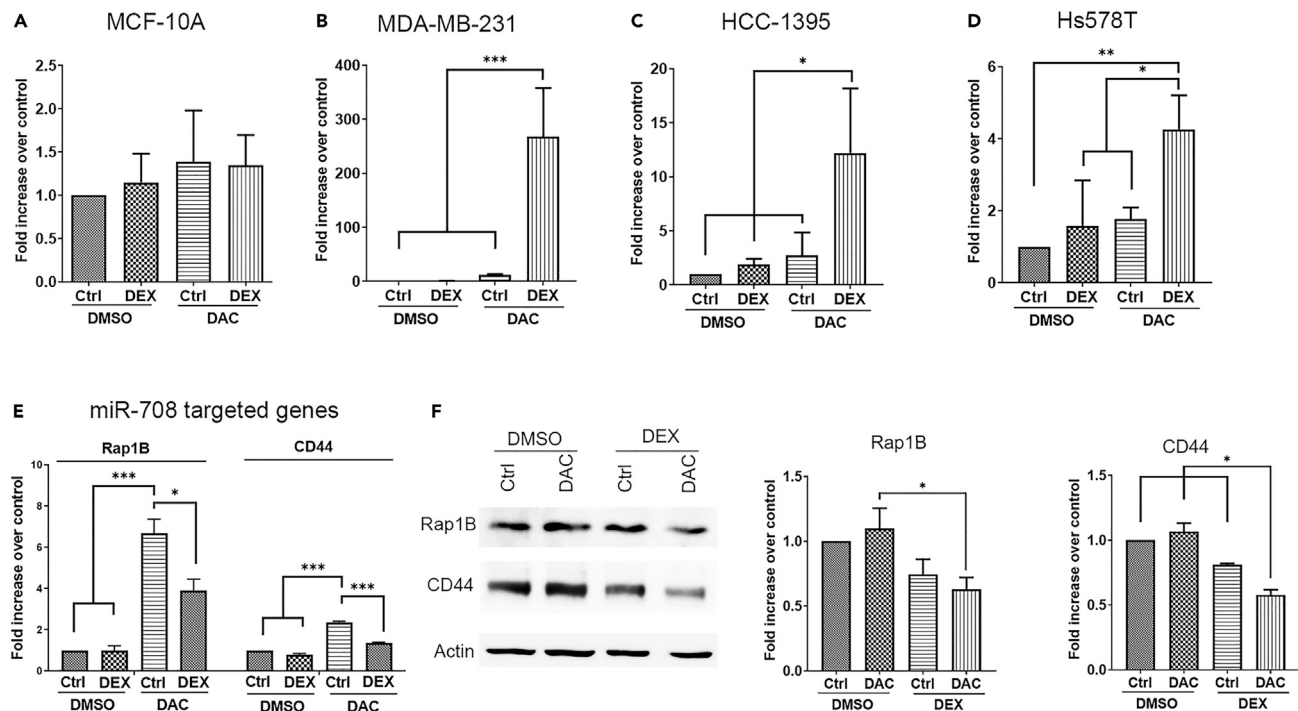


Figure 3. Treatment with DAC in combination with DEX synergistically induces the expression of miR-708 in TNBC cell lines

(A–D) Expression of miR-708 in MCF-10A (A), MDA-MB-231 (B), HCC-1395 (C), and Hs578T (D) cells after treatment with 100 nM DEX, 10 μ M DAC, or their combination for 6 days. The data shown here represent the normalized means \pm SD (n = 3 biological replicates). ANOVA followed by Tukey's post hoc test was used for the statistical analysis (*p < 0.05; **p < 0.01; ***p < 0.001).

(E) mRNA expression of the miR-708 downstream target genes Rap1B and CD44 in MDA-MB-231 cells after treatment with 100 nM DEX, 10 μ M DAC, or their combination for 6 days. The data shown here represent the normalized means \pm SD (n = 3 biological replicates). ANOVA followed by Tukey's post hoc test was used for the statistical analysis (*p < 0.05 and ***p < 0.001).

(F) Left panel: Western blot analysis of Rap1B and CD44 levels in MDA-MB-231 cells after treatment with 100 nM DEX, 10 μ M DAC, or both drugs for 6 days. Actin was used as the internal control. Right panel: Quantitative analysis of normalized Rap1B and CD44 protein levels with actin. Histograms represent normalized means \pm SEM (n = 3 biological replicates). ANOVA followed by Tukey's post hoc test was used for the statistical analysis (*p < 0.05).

groups, as observed in the principal component analysis (PCA, Figure S4B). Volcano plots showing differentially expressed genes (DEGs) in cells from different treatment groups are shown in Figure 4A.

Previous studies have already indicated that the oncogenic functions of DNMTs in TNBC include hypermethylation of the ER promoter, inhibition of apoptosis, suppression of the p53-mediated signaling pathway, and suppression of immune recognition by decreasing the expression of cancer-testis antigens (CTAs).^{42,43} By performing a gene set enrichment analysis (GSEA), we further confirmed that all these DNMT-suppressed pathways, including apoptosis, the TNF α signaling pathway, the p53 pathway, and the estrogen response pathway, were reactivated and significantly enriched (FDR < 0.25; nominal p < 0.05) in cells cotreated with DEX and DAC (Figure 4B) or DAC alone (Figure 4C). In contrast, all these pathways were not activated in cells treated with DEX alone (Data not shown). The expression of CTA genes was also induced in cells treated with DAC alone and cells cotreated with DEX and DAC (Figure S4C). Since DAC exhibits effective immune efficacy by activating CD8⁺ T cells through the induction of CTA expression in the tumor microenvironment,⁴⁴ which has been recognized as a key player in promoting breast cancer progression,⁴⁵ it is important to note that DAC can still stimulate CTA expressions when cotreated with DEX.

To evaluate the drug-drug interaction by DAC and DEX, we conducted a linear regression model with an interaction term to determine genes that are positively or negatively regulated by DAC: DEX interaction. Genes with positive interaction mean synergistic regulation by DAC and DEX, while genes with negative interaction mean antagonism between these two drugs (As illustrated in Figure 4D). The volcano plot further explored genes that were positively or negatively regulated by DAC: DEX interaction (Figure 4E). Interestingly, we observed more genes that were negatively regulated by DAC: DEX interaction with a

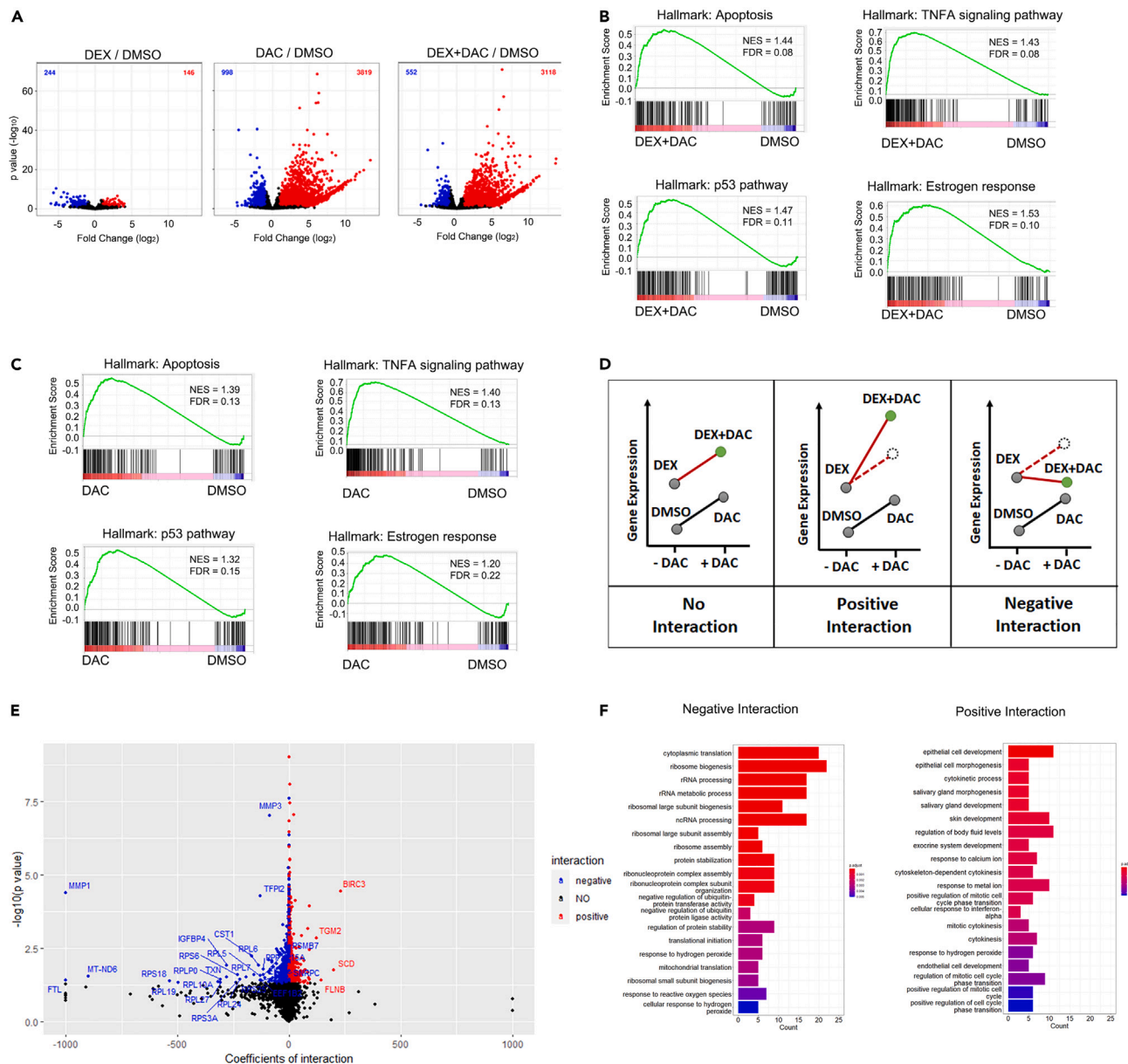


Figure 4. RNA-seq data shows differential gene expressions upon treatment with DAC, DEX, or in the combination of DAC and DEX in MDA-MB-231 cells

(A) RNA-seq analysis of MDA-MB-231 cells treated with DMSO, DAC, DEX, or both drugs for 6 days. Volcano plot showing differentially expressed genes (DEGs) from different treatment conditions. Significantly DEGs (fold change > 2) are highlighted in different colors (red for upregulated genes and blue for downregulated genes) with $p < 0.05$.

(B and C) Transcriptome data from DEX+DAC versus DMSO controls (B) or DAC versus DMSO control (C), were further analyzed using GSEA based on the latest MSigDB database for each collection. GSEA revealed the enrichment of genes associated with apoptosis, the TNF α signaling pathway, the p53 pathway, and the estrogen response. Significantly DEGs (fold change > 2) are highlighted in different colors (red for upregulated genes and blue for downregulated genes) with $p < 0.05$.

(D) Model visualization for drug interaction analysis to compare the gene expression across all treatments. If there is no interaction, the drug effects for DAC and DEX combined treatment will result solely from the addition of a single-drug effect. If there is positive interaction between DAC: DEX, the drug effects for DAC and DEX combined treatment will result in synergistic enhancement or inhibition. If there is negative interaction between DAC: DEX, the drug effects for DAC and DEX combined treatment will result in the antagonistic effect.

(E) Volcano plot of all genes with positive (shown as red) or negative (shown as blue) interactions of the two drugs (DAC: DEX; $p < 0.05$). Y axes represent the logarithm (base-10) of the p value of each coefficient of interaction. X axes represent the coefficients of interaction.

(F) GO pathway analysis from the top 100 genes ranking by the score of coefficients with negative interactions (Left) or positive interactions (Right) by DAC and DEX.

higher coefficient score, as compared to the number of genes with positive interaction (Figure 4E). We further conducted Gene Ontology (GO) and Kyoto Encyclopedia of Genes and Genomes (KEGG) pathway analyses to check the key synergistic or antagonistic responses of DAC and DEX cotreatment by applying the top 100 most affected genes (ranking by coefficient score) with positive or negative interactions ($p < 0.05$). Surprisingly, we noticed that among those genes with negative interactions, 28 of them were involved in ribosome biogenesis from both GO and KEGG pathway analyses (Figures 4F and S4D), including many large and small ribosomal proteins (the gene list is included in Table S3). Ribosome biogenesis and translational capacity are critical for cell growth and proliferation, and excessive ribosome biogenesis is commonly associated with malignant tumor behavior, therapeutic resistance, and cancer metastasis, revealing inhibition of ribosome biogenesis may have therapeutic potential against cancer development.⁴⁶ It is interesting to note that combined treatment of DAC and DEX leads to ribosome biogenesis inhibition. Further investigations will be needed to confirm this observation.

The combined regimen of DEX and DAC impairs the expression of genes related to distant metastasis

We then compared the DEGs between cells treated with DEX+DAC or DAC alone to identify other important pathways modified by the combined treatment with DEX and DAC. A heatmap analysis showed all upregulated and downregulated DEGs between the DEX+DAC and DAC groups (fold change ≥ 2) among all samples (Figure S5). Interestingly, we observed that the expression of some genes involved in cancer invasion and distant metastasis was significantly induced in DAC-treated cells and downregulated in cells cotreated with DEX and DAC, including matrix metalloproteinases (MMPs) 1, 3, 9, 13, and interleukin-1 β (IL-1 β). Consistently, we also observed expressions of these genes were negatively interacted by DAC: DEX treatment (Table S3), especially MMP1 (Figure 4E). GSEA profiles further indicated a negative correlation of genes involved in the collagen catabolic process and cytokine and cytokine receptor interactions between the cotreated group and the group treated with DAC alone (Figures 5A and 5B), revealing that the expression of genes involved in the extracellular matrix (ECM) remodeling and inflammation was suppressed by cotreatment with DEX and DAC compared with the DAC treatment alone. The expression of these genes was further validated through RT-qPCR in MDA-MB-231 and HCC-1395 cells (Figure 5C). Since MMP1, MMP3, MMP9, and IL-1 β are known NF- κ B targeted genes^{47–50} to promote cancer cell invasion and distant metastasis,^{51–53} it is possible that the cotreatment with DEX potentially suppresses DAC-induced transcription on NF- κ B targeted genes through transrepression regulation by the glucocorticoid receptor (GR).⁵⁴ To further address whether NF- κ B signaling is upregulated by DAC and further repressed by DEX cotreatment, we applied a luciferase vector with 4X NF- κ B response element to access NF- κ B activity. Here our data indicated that NF- κ B activity was up-regulated by DAC treatment, and this induction was further reduced by DEX cotreatment (Figure 5D), confirming that DEX-cotreatment can inhibit DAC-induced expressions of MMPs and IL-1 β through inhibition of NF- κ B activity. Overall, our data reveal that cotreatment of DAC with DEX not only retains the activities of DAC by blocking DNA methylation to achieve growth inhibition and immune recognition in these cancer cells but suppresses expressions of metastatic promoting genes induced by DAC.

The combined regimen of DEX and DAC inhibits the proliferation, migration, and invasion of TNBC cells

We examined cell proliferation, migration, and invasion in the presence of DEX and DAC to further assess the effects of these two drugs on cellular functions. The cell proliferation rate was reduced in the presence of DAC and cotreatment with DEX and DAC in MDA-MB-231 (Figure 6A) and HCC-1395 cells (Figure S6A), suggesting that cell proliferation can be suppressed by DAC alone. In contrast, the combination of these two drugs reduced the migration and invasion compared to any of the single drug treatments alone in MDA-MB-231 (Figures 6B and 6C) and HCC-1395 cells (Figures S6B and S6C). We further elucidated the direct function of miR-708 in TNBC cells. The cell proliferation was not affected by miR-708 expression while both cell migration and invasion were greatly reduced in cells overexpressing miR-708 in both MDA-MB-231 (Figures 6D–6F) and HCC-1395 cells (Figures S6D–S6F), suggesting miR-708 is an effective suppressor for motility and invasion. To assess whether the suppressive effects we observed in the cotreatment group (Figures 6A–6C and S6A–S6C) were mainly or partially mediated by miR-708, we overexpressed anti-miR-708 (anti-708) in cells before treatment with DEX and DAC. As expected, expression of anti-708 cannot rescue cotreatment-induced inhibition of cell proliferation in both MDA-MB-231 (Figure 6G) and HCC-1395 cells (Figure S6G). Meanwhile, expression of anti-708 can partially or completely rescue cotreatment-reduced cell migration and invasion in MDA-MB-231 (Figures 6H and 6I) or HCC-1395 (Figures S6H and S6I), respectively. The partial rescue we observed in MDA-MB-231 cells suggests that

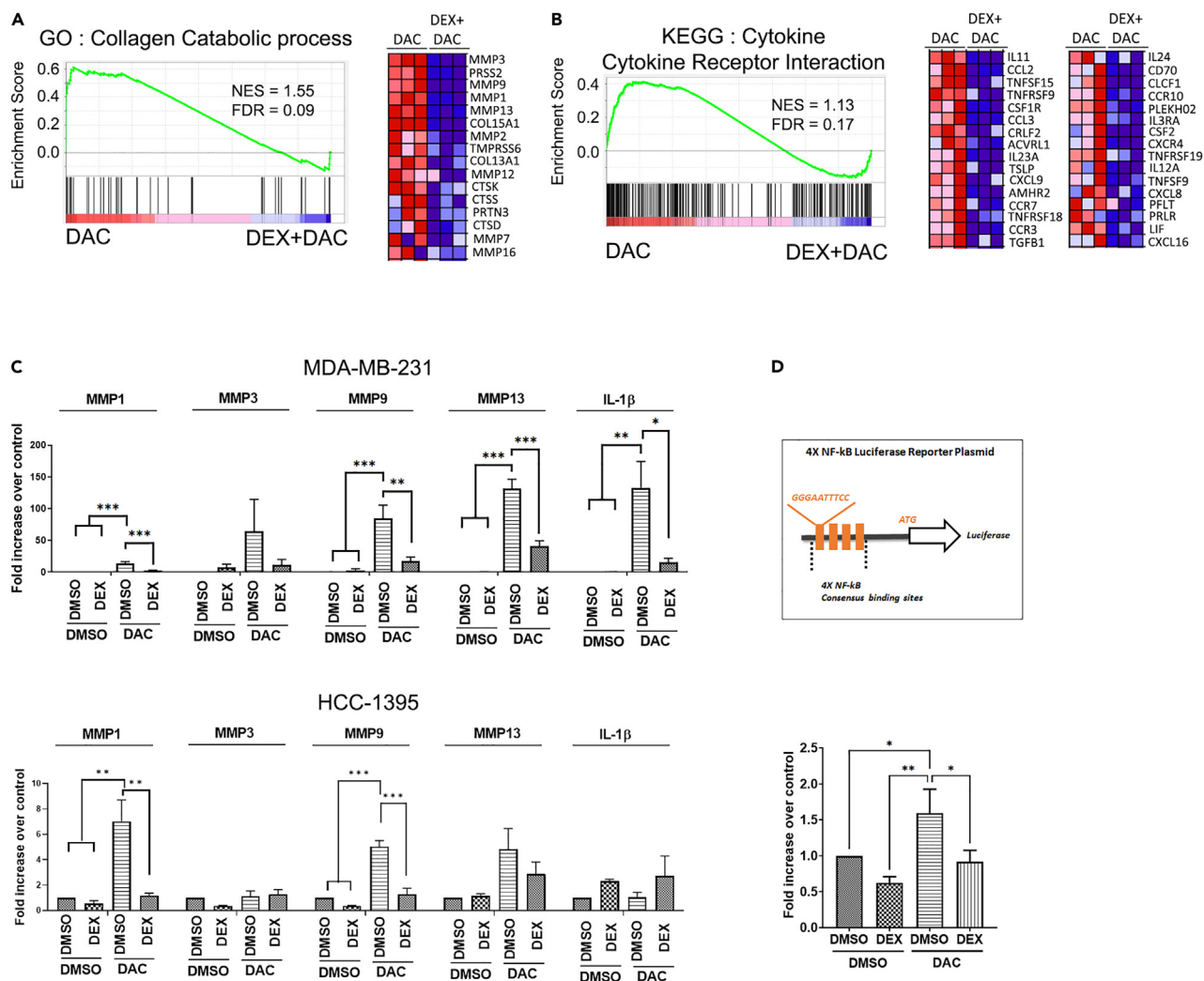


Figure 5. Treatment with DAC in combination with DEX impairs genes involved in promoting distant metastasis

(A and B) Left panel: Transcriptome data from the DEX+DAC and DAC groups were further analyzed using GSEA based on the latest MSigDB database for each collection. The GSEA revealed the enrichment of genes associated with the Gene Ontology pathway: Collagen catabolic process (A) and KEGG pathway: Cytokine-cytokine receptor interaction (B). Left: Significantly DEGs (fold change > 2) are highlighted in different colors (red for upregulated genes and blue for downregulated genes) with $p < 0.05$. Right: A heatmap showing the dynamic expression of the core enriched genes involved in these two signaling pathways. (C) RT-qPCR analyses validated the DEGs between the DEX+DAC and DAC groups identified from the RNA-seq data. MDA-MB-231 and HCC-1395 cells were treated with 100 nM DEX alone or in combination with 10 μ M DAC for 6 days. The expression of MMP1, 3, 9, 13, and IL-1 β was analyzed. Data shown here represent the normalized means \pm SD ($n = 3$ biological replicates). ANOVA followed by Tukey's post hoc test was used for the statistical analysis (* $p < 0.05$; ** $p < 0.01$; and *** $p < 0.001$).

(D) Top: Schematic diagram of 4X NF- κ B-responsive firefly luciferase reporter plasmid. Bottom: MDA-MB-231 cells were transfected with the NF- κ B-responsive firefly luciferase reporter and GFP as the internal control for 24 h. Cells were then incubated with DMSO, DAC (1 μ M), or DEX (100 nM) for another 24 h. The data shown here represent the normalized luciferase activity \pm SD ($n = 3$ biological replicates). ANOVA followed by Tukey's post hoc test was used for the statistical analysis (* $p < 0.05$; ** $p < 0.01$).

DEX and DAC cotreatment may not only induce miR-708 expression (Figure 3B) but also inhibit expressions of other metastatic genes (Figure 5C). Both pathways contribute to the significant suppression of cell migration and invasion in MDA-MB-231 cells cotreated with DEX and DAC.

The combined regimen of DEX and DAC significantly suppresses tumor growth and metastasis in a TNBC xenograft mouse model

MDA-MB-231 cell-derived breast cancer xenograft models were applied to test whether the combined regimen of DEX and DAC exerted suppressive effects on breast cancer progression and metastasis. We

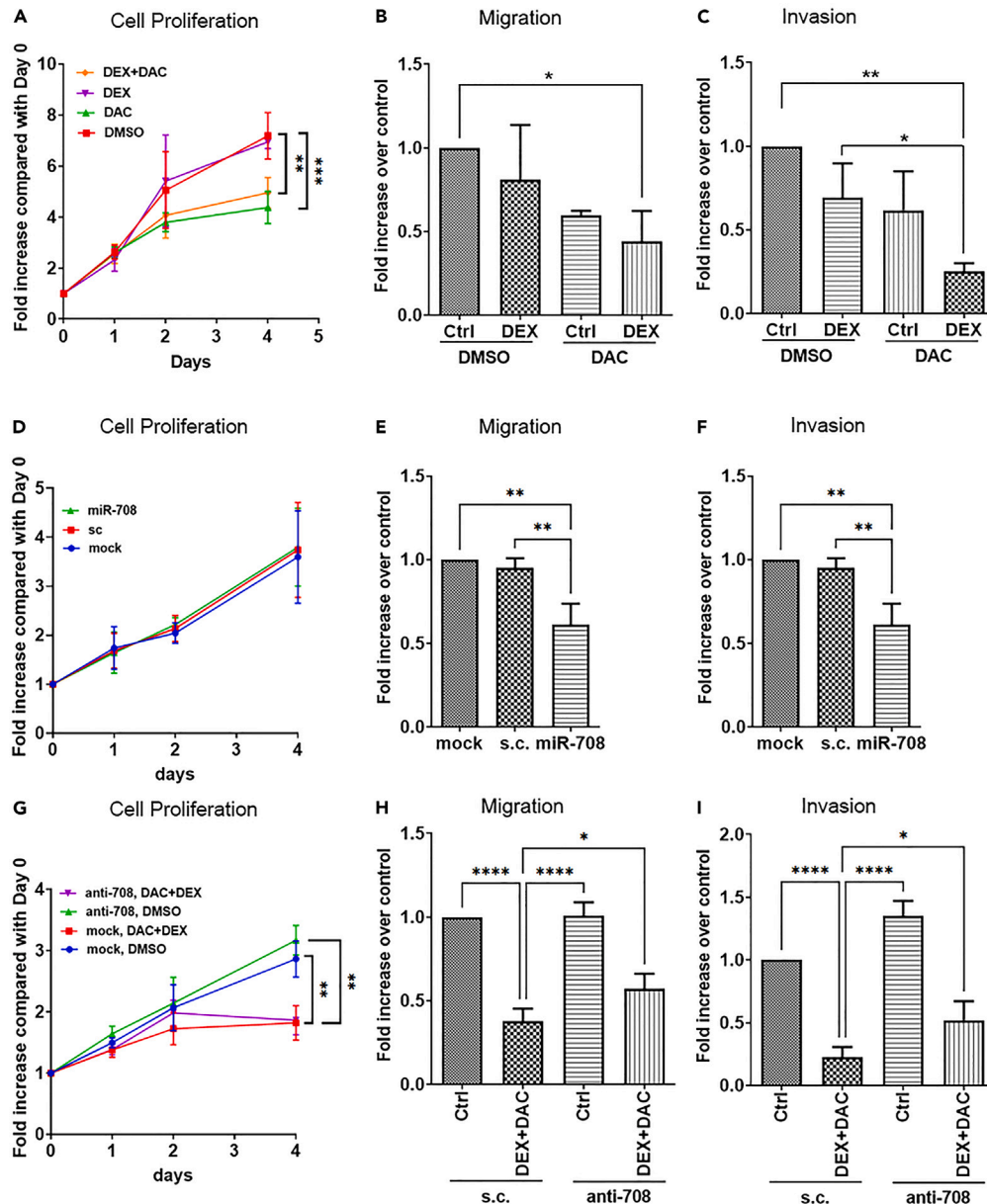


Figure 6. Treatment with DAC in combination with DEX inhibits the proliferation, migration, and invasion of MDA-MB-231 cells

(A) Cell proliferation assays were performed after treatment with DEX, DAC, or DMSO control in MDA-MB-231 cells with MTS reagent. Data are presented as the means \pm SD (n = 3 biological replicates).

(B and C) MDA-MB-231 cells were treated with DEX alone or in combination with DAC for three days and then incubated for migration (B) and invasion (C) assays. DMEM/10% fetal bovine serum (FBS), together with DEX or DAC, served as a chemoattractant. The data shown here represent the normalized means \pm SD (n = 3 biological replicates).

(D) Cell proliferation assays were performed after 24 h transfection of miR-708 in MDA-MB-231 cells with MTS reagent. Data are presented as the means \pm SD (n = 3 biological replicates).

(E and F) MDA-MB-231 cells were transfected with miR-708 for 48 h and then incubated for migration (E) and invasion (F) assays. DMEM/10% FBS served as a chemoattractant. The data shown here represent the normalized means \pm SD (n = 3 biological replicates).

(G) Cell proliferation assays were performed after transfection with anti-miR-708 for 24 h and then treatment with DEX, DAC, or DMSO control in MDA-MB-231 cells by using an MTS reagent. Data are presented as the means \pm SD (n = 3 biological replicates).

Figure 6. Continued

(H and I) MDA-MB-231 cells were transfected with anti-miR-708 for 24 h, treated with DEX alone or in combination with DAC for another 24 h, and then incubated for migration (H) and invasion (I) assays. DMEM/10% FBS, together with DEX or DAC, served as a chemoattractant. The data shown here represent the normalized means \pm SD (n = 3 biological replicates).

(A, D, and G) One-way ANOVA followed by Tukey's post hoc test was used for the statistical analysis on the last day (**p < 0.01; ***p < 0.001).

(B, C, E, F, H, and I) One-way ANOVA followed by Tukey's post hoc test was used for the statistical analysis (*p < 0.05; **p < 0.01; ***p < 0.001; ****p < 0.0001).

observed a significant decrease in tumor growth in xenografts from mice cotreated with DEX and DAC compared with the vehicle control (Figures 7A–7C). The mouse body weights remained similar among all groups (Figure 7D). The tumor volume and distant metastases were determined using *in vivo* bioluminescent (IVIS) imaging (Figure 7E). Multiple preferential metastatic organs of breast cancer, including axillary lymph nodes, lung, liver, and spinal cord, were collected for *ex vivo* bioluminescent imaging (Figure 7F). Both the incidence and the size of metastatic tumors in lung and lymph node metastases were suppressed only in the group administered the combined treatment (Figures 7G and 7H), suggesting DEX and DAC cotreatment synergistically induced genes, such as miR-708, involved in the suppression of cancer metastasis. Overall, our data suggest that the combination treatment with DEX and DAC significantly suppresses breast tumor growth and distant metastasis in an MDA-MB-231-derived TNBC xenograft model, revealing the potential of using this combined regimen for future TNBC targeted therapy.

DISCUSSION

Aberrant DNA methylation at CpG sites is one of the epigenetic mechanisms that contribute to breast cancer progression by silencing tumor suppressor genes.⁵ The DNMT inhibitor DAC has been tested in clinical trials to treat breast cancer, especially TNBC, for which no targeted therapies are currently available. Here we propose to use the combined regimen of DEX and DAC to inhibit tumor growth and cancer metastasis for TNBC-targeted therapy. We identified three leading pathways stimulated by the combined treatment of DAC and DEX. At first, cotreatment of DAC and DEX reactivates the expression of genes related to apoptosis, ER response, p53 pathways, and CTAs (Figures 4B, 4C, and S4C), consistent with previous observations found in DAC studies.⁴² Second, treatment with DAC stimulates NF- κ B response genes, including MMPs and IL-1 β . These inductions can be further suppressed by DEX-mediated GR-transrepression on NF- κ B activity⁵⁵ (Figure 5D). Third, we observed that the combination of these two drugs synergistically increases miR-708 expression to higher levels in TNBC cell lines (Figures 3B–3D), resulting in the significant suppression of cell migration and invasion (Figures 6 and S6). With all these three distinct pathways, the combined treatment of DEX and DAC significantly suppressed tumor growth and distant metastasis in an MDA-MB-231 xenograft mouse model.

DEX, a widely prescribed synthetic GC with high safety and relatively few side effects, is often used to relieve the negative effects caused by chemotherapy on patients with breast cancer.³³ However, whether GC promotes or inhibits tumor progression is controversial in breast cancer and other non-hematologic cancer types.⁵⁴ GC has been linked to anti-apoptosis and results in resistance to chemotherapy-induced breast cancer cell death.^{56,57} Aberrant GR activation in ER-negative breast cancer promotes epithelial-mesenchymal transition (EMT) progress⁵⁸ and distant metastasis.³⁴ However, these observations are not yet proved clinically. In contrast, a recent large epidemiological study reveals that breast cancer patients, regardless of whether ER-positive or ER-negative, who receiving GC as adjuvant chemotherapy showed longer breast cancer-specific survival, as compared with those without GC cotreatment, suggesting the use of GC may be beneficial for the net outcome of breast cancer patients.³⁶ Moreover, our previous study reveals an interesting phenomenon that treatment with DEX at a low dose (5 μ g/kg) suppressed breast cancer progression in the MCF-7 or MDA-MB-231 xenograft mouse model, while treatment with high-dose DEX (50 μ g/kg) stimulates both tumor growth and distant metastasis,²⁷ revealing that the importance of determining the optimal dose and duration of GC while treating breast-cancer patients because different doses may result in opposite consequences.

Previous studies have provided strong evidence that miR-708 functions as a tumor suppressor in metastatic breast cancer.¹⁶ Here, we observed that the expression of miR-708 is highly downregulated in TNBC tumors and metastatic LNs (Figure 1B), and low miR-708 expression is correlated with poor survival in patients with TNBC (Figure 1D), indicating that miR-708 may represent as a great prognostic marker and therapeutic

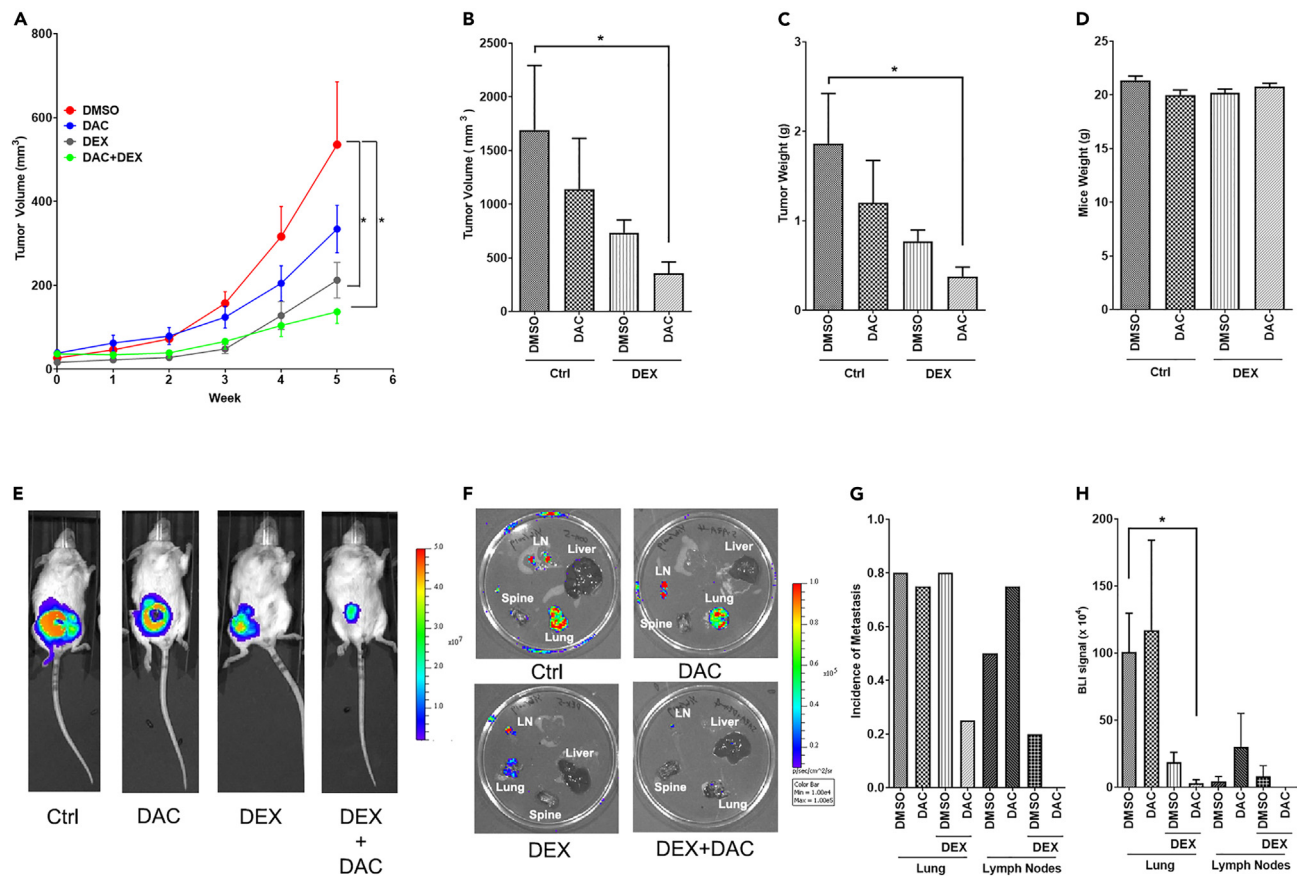


Figure 7. The regimen combining DEX and DAC suppresses both tumor growth and metastasis in a TNBC xenograft mouse model

MDA-MB-231 cells stably expressing luciferase (2×10^6) were orthotopically injected into the fourth mammary fat pads. Five days after implantation, intraperitoneal injections of DEX (5 $\mu\text{g}/\text{kg}$) and DAC (50 $\mu\text{g}/\text{kg}$) were started three times a week until the endpoint. (A–D) Tumor growth (A) was monitored weekly. Tumor volume (B), tumor weight (C), and mice weight (D) were compared at the endpoint. Data are presented as the means \pm SEM ($n = 8\text{--}11$; data were combined from two separate experiments). One-way ANOVA followed by Tukey's post hoc test was used for the statistical analysis ($*p < 0.05$).

(E) The kinetics of tumor growth was monitored using *in vivo* bioluminescence imaging (BLI).

(F) Individual organ metastases, including lung, liver, spine, and lymph node (LN) metastases, were monitored using *ex vivo* BLI.

(G and H) The incidence (G) and quantification (H) of lung and axillary lymph node metastases were obtained from BLI measurements. Data are presented as means \pm SEM ($n = 4\text{--}5$ per group). One-way ANOVA followed by Tukey's post hoc test was used for the statistical analysis ($*p < 0.05$).

target for patients with TNBC. The delivery of miR-708 through nanoparticles has been considered an RNAi-based targeted therapy for TNBC.³¹ However, RNAi-based drug delivery is still a challenging issue. The main barriers are endosomal escape, delivery of an optimal amount of the drug, and toxicity caused by nanoparticles.⁵⁹ In contrast, our strategy provides a more efficient and safer method to stimulate miR-708 expression in TNBC cells (Figures 3B–3D). Moreover, DAC alone suppresses cell proliferation and tumor growth in multiple cancer types, including MDA-MB-231 cells.⁶⁰ Here, our data confirmed the observations of previous studies (Figures 4C and S4C), and the regimen combining DAC and DEX showed more significant suppression of tumor growth and distant metastasis (Figure 7).

Studies have shown that miR-708 targets Rap1B, CD44, and IKK β directly.^{17,18,23} Here our data indicated that mRNA levels of these three genes were not as expected to be significantly reduced to basal level in cells cotreated with DAC and DEX (Figures 3E and S3C). In contrast, the protein levels of Rap1B, CD44, and IKK β were all down-regulated in cells cotreated with DAC and DEX, as compared to the DMSO control (Figures 3F and S3D). Since microRNA not only can decrease mRNA stability but also inhibit protein translation machinery. Therefore, the miR-708 induction by cotreatment (Figure 3B) may further suppress protein translation efficiency on Rap1B, CD44 (Figure 3F), and IKK β (Figure S3D). On the other hand, our

RNAseq analysis elucidated that genes involved in the ribosome biogenesis were negatively regulated by DAC and DEX interactions (Figures 4E and 4F), resulting in the significant suppression of gene expressions. Since this inhibition may interfere with protein translation,⁴⁶ we suspect that the inhibition of protein levels on Rap1B, CD44, and IKK β by cotreatment may also be related to the inhibition of ribosome biogenesis.

In addition to DNA hypomethylating drugs, such as DAC, histone deacetylase (HDAC) inhibitors and histone methyltransferase (HMT) inhibitors are considered other approaches to target epigenetic modifications in TNBC.^{61,62} Notably, recent reports indicate that enhancer of zeste homolog 2 (EZH2), one of the HMTs, plays an important role in the suppression of miR-708 expression during cancer development in breast cancer,¹⁶ prostate cancer,²⁶ and glioma,²⁵ revealing a potential opportunity to combine DEX with EZH2 inhibitors to increase miR-708 expression. Based on this knowledge, combinations of epi-drugs, such as DAC, with DEX may represent a better therapeutic option to treat patients with TNBC.

In summary, our study indicates that combined treatment of DNA-demethylating agent DAC and synthetic GC, DEX, work together to suppress tumor growth and distant metastasis in the TNBC. Since both DEX and DAC are FDA-approved drugs with confirmed safety and effectiveness, we hope our strategy against TNBC will be rapidly developed soon to benefit more patients.

Limitations of the study

Despite having provided compelling evidence that combination treatment with the hypomethylating agent decitabine and synthetic glucocorticoid significantly increased the expression of microRNA-708, re-activated DNMT-suppressed pathways, and decreased the expression of multiple metastasis-promoting genes to suppress TNBC, however, how the combination of these two drugs may impact normal tissues remains unknown. More work will be needed to dissect how decitabine together with glucocorticoid may affect the human body, especially our immune system.

STAR★METHODS

Detailed methods are provided in the online version of this paper and include the following:

- KEY RESOURCES TABLE
- RESOURCE AVAILABILITY
 - Lead contact
 - Materials availability
 - Data and code availability
- EXPERIMENTAL MODEL AND SUBJECT DETAILS
 - Animals
 - Human samples
 - Cell lines
- METHOD DETAILS
 - Transfection
 - Nucleotides and reagents
 - Quantitative real-time PCR analysis of mRNAs and miRNAs
 - Western blot analysis
 - Transwell cell migration and cell invasion assays
 - Cell proliferation assay
 - Bisulfite sequencing
 - *In vivo* xenograft mouse model
 - RNA-seq analysis
 - Kaplan–Meier plotter database analysis
 - Retrieving miRNA-seq and methylation array data from The Cancer Genome Atlas
- QUANTIFICATION AND STATISTICAL ANALYSIS

SUPPLEMENTAL INFORMATION

Supplemental information can be found online at <https://doi.org/10.1016/j.isci.2023.106597>.

ACKNOWLEDGMENTS

This work was supported by the National Science and Technology Council (MSTC), Taiwan (105-2321-B-007-008-MY3, 107-2320-B-007-003-MY3, 108-2314-B-007-003-MY3, and 111-2320-B-007-005-MY3) and National Tsing Hua University (111Q2713E1, 112Q2511E1, and 112Q2521E1). We thank Dr. Li-Chung Hsu from National Taiwan University for providing us with the 4X NF- κ B-responsive firefly luciferase reporter plasmid as a kind gift.

AUTHOR CONTRIBUTIONS

Y.C., Y.H., P.C., Y.P., Y.K., R.W., Y.K., Y.W., and K.L. carried out the experimental work. W.K. provided clinical samples and clinical aspects of suggestions. P.C., Y.C., and Y.L. conducted the bioinformatic analysis. K.L. designed experiments, wrote the manuscript, directed the research, and approved the manuscript.

DECLARATION OF INTERESTS

The authors declare that they have no conflicts of interest with the contents of this article.

Received: August 18, 2022

Revised: December 9, 2022

Accepted: April 3, 2023

Published: April 8, 2023

REFERENCES

- Polyak, K. (2011). Heterogeneity in breast cancer. *J. Clin. Invest.* *121*, 3786–3788. <https://doi.org/10.1172/JCI60534>.
- Xu, H., Eirew, P., Mullaly, S.C., and Aparicio, S. (2014). The omics of triple-negative breast cancers. *Clin. Chem.* *60*, 122–133. <https://doi.org/10.1373/clinchem.2013.207167>.
- Feng, Y., Spezia, M., Huang, S., Yuan, C., Zeng, Z., Zhang, L., Ji, X., Liu, W., Huang, B., Luo, W., et al. (2018). Breast cancer development and progression: Risk factors, cancer stem cells, signaling pathways, genomics, and molecular pathogenesis. *Genes Dis.* *5*, 77–106. <https://doi.org/10.1016/j.gendis.2018.05.001>.
- Jones, P.A., and Baylin, S.B. (2007). The epigenomics of cancer. *Cell* *128*, 683–692. <https://doi.org/10.1016/j.cell.2007.01.029>.
- Jovanovic, J., Rønneberg, J.A., Tost, J., and Kristensen, V. (2010). The epigenetics of breast cancer. *Mol. Oncol.* *4*, 242–254. <https://doi.org/10.1016/j.molonc.2010.04.002>.
- Cheng, Y., He, C., Wang, M., Ma, X., Mo, F., Yang, S., Han, J., and Wei, X. (2019). Targeting epigenetic regulators for cancer therapy: mechanisms and advances in clinical trials. *Signal Transduct. Target. Ther.* *4*, 62. <https://doi.org/10.1038/s41392-019-0095-0>.
- Christman, J.K. (2002). 5-Azacytidine and 5-aza-2'-deoxycytidine as inhibitors of DNA methylation: mechanistic studies and their implications for cancer therapy. *Oncogene* *21*, 5483–5495.
- Döhner, H., Estey, E., Grimwade, D., Amadori, S., Appelbaum, F.R., Büchner, T., Dombret, H., Ebert, B.L., Fenaux, P., Larson, R.A., et al. (2017). Diagnosis and management of AML in adults: 2017 ELN recommendations from an international expert panel. *Blood* *129*, 424–447. <https://doi.org/10.1182/blood-2016-08-733196>.
- Bohl, S.R., Bullinger, L., and Rücker, F.G. (2018). Epigenetic therapy: azacytidine and decitabine in acute myeloid leukemia. *Expert Rev. Hematol.* *11*, 361–371. <https://doi.org/10.1080/17474086.2018.1453802>.
- Cowan, L.A., Talwar, S., and Yang, A.S. (2010). Will DNA methylation inhibitors work in solid tumors? A review of the clinical experience with azacitidine and decitabine in solid tumors. *Epigenomics* *2*, 71–86. <https://doi.org/10.2217/epi.09.44>.
- Fu, S., Hu, W., Iyer, R., Kavanagh, J.J., Coleman, R.L., Levenback, C.F., Sood, A.K., Wolf, J.K., Gershenson, D.M., Markman, M., et al. (2011). Phase 1b-2a study to reverse platinum resistance through use of a hypomethylating agent, azacitidine, in patients with platinum-resistant or platinum-refractory epithelial ovarian cancer. *Cancer* *117*, 1661–1669. <https://doi.org/10.1002/cncr.25701>.
- Singal, R., Ramachandran, K., Gordian, E., Quintero, C., Zhao, W., and Reis, I.M. (2015). Phase I/II study of azacitidine, docetaxel, and prednisone in patients with metastatic castration-resistant prostate cancer previously treated with docetaxel-based therapy. *Clin. Genitourin. Cancer* *13*, 22–31. <https://doi.org/10.1016/j.clgc.2014.07.008>.
- Yu, J., Qin, B., Moyer, A.M., Nowsheen, S., Liu, T., Qin, S., Zhuang, Y., Liu, D., Lu, S.W., Kalari, K.R., et al. (2018). DNA methyltransferase expression in triple-negative breast cancer predicts sensitivity to decitabine. *J. Clin. Invest.* *128*, 2376–2388. <https://doi.org/10.1172/JCI97924>.
- Lee, Y.S., and Dutta, A. (2009). MicroRNAs in cancer. *Annu. Rev. Pathol.* *4*, 199–227. <https://doi.org/10.1146/annurev.pathol.4.110807.092222>.
- Peng, Y., and Croce, C.M. (2016). The role of MicroRNAs in human cancer. *Signal Transduct. Target. Ther.* *1*, 15004. <https://doi.org/10.1038/sigtrans.2015.4>.
- Ryu, S., McDonnell, K., Choi, H., Gao, D., Hahn, M., Joshi, N., Park, S.M., Catena, R., Do, Y., Brazin, J., et al. (2013). Suppression of miRNA-708 by polycomb group promotes metastases by calcium-induced cell migration. *Cancer Cell* *23*, 63–76. <https://doi.org/10.1016/j.ccr.2012.11.019>.
- Lin, K.T., Yeh, Y.M., Chuang, C.M., Yang, S.Y., Chang, J.W., Sun, S.P., Wang, Y.S., Chao, K.C., and Wang, L.H. (2015). Glucocorticoids mediate induction of microRNA-708 to suppress ovarian cancer metastasis through targeting Rap1B. *Nat. Commun.* *6*, 5917. <https://doi.org/10.1038/ncomms6917>.
- Saini, S., Majid, S., Shahryari, V., Arora, S., Yamamura, S., Chang, I., Zaman, M.S., Deng, G., Tanaka, Y., and Dahiya, R. (2012). miRNA-708 control of CD44(+) prostate cancer-initiating cells. *Cancer Res.* *72*, 3618–3630. <https://doi.org/10.1158/0008-5472.CAN-12-0540>.
- Song, T., Zhang, X., Zhang, L., Dong, J., Cai, W., Gao, J., and Hong, B. (2013). miR-708 promotes the development of bladder carcinoma via direct repression of Caspase-2. *J. Cancer Res. Clin. Oncol.* *139*, 1189–1198. <https://doi.org/10.1007/s00432-013-1392-6>.
- Wu, X., Liu, T., Fang, O., Dong, W., Zhang, F., Leach, L., Hu, X., and Luo, Z. (2016). MicroRNA-708-5p acts as a therapeutic agent against metastatic lung cancer. *Oncotarget* *7*, 2417–2432. <https://doi.org/10.18632/oncotarget.6594>.

21. Saini, S., Yamamura, S., Majid, S., Shahyari, V., Hirata, H., Tanaka, Y., and Dahiya, R. (2011). MicroRNA-708 induces apoptosis and suppresses tumorigenicity in renal cancer cells. *Cancer Res.* 71, 6208–6219. <https://doi.org/10.1158/0008-5472.CAN-11-0073>.
22. Li, Q., Li, S., Wu, Y., and Gao, F. (2017). miRNA-708 functions as a tumour suppressor in hepatocellular carcinoma by targeting SMAD3. *Oncol. Lett.* 14, 2552–2558. <https://doi.org/10.3892/ol.2017.6429>.
23. Baer, C., Oakes, C.C., Ruppert, A.S., Claus, R., Kim-Wanner, S.Z., Mertens, D., Zenz, T., Stilgenbauer, S., Byrd, J.C., and Plass, C. (2015). Epigenetic silencing of miR-708 enhances NF-kappaB signaling in chronic lymphocytic leukemia. *Int. J. Cancer* 137, 1352–1361. <https://doi.org/10.1002/ijc.29491>.
24. Baer, C., Claus, R., Frenzel, L.P., Zucknick, M., Park, Y.J., Gu, L., Weichenhan, D., Fischer, M., Pallasch, C.P., Herpel, E., et al. (2012). Extensive promoter DNA hypermethylation and hypomethylation is associated with aberrant microRNA expression in chronic lymphocytic leukemia. *Cancer Res.* 72, 3775–3785. <https://doi.org/10.1158/0008-5472.CAN-12-0803>.
25. Chen, Y., Deng, X., Chen, W., Shi, P., Lian, M., Wang, H., Wang, K., Qian, D., Xiao, D., and Long, H. (2019). Silencing of microRNA-708 promotes cell growth and epithelial-to-mesenchymal transition by activating the SPHK2/AKT/beta-catenin pathway in glioma. *Cell Death Dis.* 10, 448. <https://doi.org/10.1038/s41419-019-1671-5>.
26. Shan, J., Al-Muftah, M.A., Al-Kowari, M.K., Abuaqel, S.W.J., Al-Rumaihi, K., Al-Bozom, I., Li, P., and Chouchane, L. (2019). Targeting Wnt/EZH2/microRNA-708 signaling pathway inhibits neuroendocrine differentiation in prostate cancer. *Cell Death Discov.* 5, 139. <https://doi.org/10.1038/s41420-019-0218-y>.
27. Pang, J.M., Huang, Y.-C., Sun, S.-P., Pan, Y.-R., Shen, C.-Y., Kao, M.-C., Wang, R.-H., Wang, L.-H., and Lin, K.-T. (2020). Effects of synthetic glucocorticoids on breast cancer progression. *Steroids*, 108738.
28. Senthil Kumar, K.J., Gokila Vani, M., Hsieh, H.W., Lin, C.C., Liao, J.W., Chueh, P.J., and Wang, S.Y. (2019). MicroRNA-708 activation by glucocorticoid receptor agonists regulate breast cancer tumorigenesis and metastasis via downregulation of NF-kappaB signaling. *Carcinogenesis* 40, 335–348. <https://doi.org/10.1093/carcin/bgz011>.
29. Ma, L., Ma, S., Zhao, G., Yang, L., Zhang, P., Yi, Q., and Cheng, S. (2016). miR-708/LSD1 axis regulates the proliferation and invasion of breast cancer cells. *Cancer Med.* 5, 684–692. <https://doi.org/10.1002/cam4.623>.
30. Nygren, M.K., Tekle, C., Ingebrigtsen, V.A., Mäkelä, R., Krohn, M., Aure, M.R., Nunes-Xavier, C.E., Perälä, M., Tramm, T., Alsner, J., et al. (2014). Identifying microRNAs regulating B7-H3 in breast cancer: the clinical impact of microRNA-29c. *Br. J. Cancer* 110, 2072–2080. <https://doi.org/10.1038/bjc.2014.113>.
31. Ramchandani, D., Lee, S.K., Yomtoubian, S., Han, M.S., Tung, C.H., and Mittal, V. (2019). Nanoparticle delivery of miR-708 Mimetic impairs breast cancer metastasis. *Mol. Cancer Ther.* 18, 579–591. <https://doi.org/10.1158/1535-7163.MCT-18-0702>.
32. Oster, H., Challet, E., Ott, V., Arvat, E., de Kloet, E.R., Dijk, D.J., Lightman, S., Vgontzas, A., and Van Cauter, E. (2017). The functional and clinical significance of the 24-Hour Rhythm of Circulating glucocorticoids. *Endocr. Rev.* 38, 3–45. <https://doi.org/10.1210/er.2015-1080>.
33. Pufall, M.A. (2015). Glucocorticoids and cancer. *Adv. Exp. Med. Biol.* 872, 315–333. https://doi.org/10.1007/978-1-4939-2895-8_14.
34. Obradović, M.M.S., Hamelin, B., Manevski, N., Couto, J.P., Sethi, A., Coissieux, M.M., Müst, S., Okamoto, R., Kohler, H., Schmidt, A., and Bentires-Alj, M. (2019). Glucocorticoids promote breast cancer metastasis. *Nature* 567, 540–544. <https://doi.org/10.1038/s41586-019-1019-4>.
35. Lietzen, L.W., Ahern, T., Christiansen, P., Jensen, A.B., Sørensen, H.T., Lash, T.L., and Cronin-Fenton, D.P. (2014). Glucocorticoid prescriptions and breast cancer recurrence: a Danish nationwide prospective cohort study. *Ann. Oncol.* 25, 2419–2425. <https://doi.org/10.1093/annonc/mdu453>.
36. Lin, C.H., Chuang, P.Y., You, S.L., Chiang, C.J., Huang, C.S., Wang, M.Y., Chao, M., Lu, Y.S., Cheng, A.L., and Tang, C.H. (2018). Effect of glucocorticoid use on survival in patients with stage I-III breast cancer. *Breast Cancer Res. Treat.* 171, 225–234. <https://doi.org/10.1007/s10549-018-4787-x>.
37. Monteleone, N.J., and Lutz, C.S. (2017). miR-708-5p: a microRNA with emerging roles in cancer. *Oncotarget* 8, 71292–71316. <https://doi.org/10.18632/oncotarget.19772>.
38. Esteller, M. (2002). CpG island hypermethylation and tumor suppressor genes: a booming present, a brighter future. *Oncogene* 21, 5427–5440. <https://doi.org/10.1038/sj.onc.1205600>.
39. Díez-Villanueva, A., Mallona, I., and Peinado, M.A. (2015). Wanderer, an interactive viewer to explore DNA methylation and gene expression data in human cancer. *Epigenet. Chromatin* 8, 22. <https://doi.org/10.1186/s13072-015-0014-8>.
40. Yin, L., Duan, J.J., Bian, X.W., and Yu, S.C. (2020). Triple-negative breast cancer molecular subtyping and treatment progress. *Breast Cancer Res.* 22, 61. <https://doi.org/10.1186/s13058-020-01296-5>.
41. Greten, F.R., Eckmann, L., Greten, T.F., Park, J.M., Li, Z.W., Egan, L.J., Kagnoff, M.F., and Karin, M. (2004). IKKbeta links inflammation and tumorigenesis in a mouse model of colitis-associated cancer. *Cell* 118, 285–296. <https://doi.org/10.1016/j.cell.2004.07.013>.
42. Wong, K.K. (2021). DNMT1: a key drug target in triple-negative breast cancer. *Semin. Cancer Biol.* 72, 198–213. <https://doi.org/10.1016/j.semcancer.2020.05.010>.
43. Simpson, A.J.G., Caballero, O.L., Jungbluth, A., Chen, Y.T., and Old, L.J. (2005). Cancer/testis antigens, gametogenesis and cancer. *Nat. Rev. Cancer* 5, 615–625. <https://doi.org/10.1038/nrc1669>.
44. Li, X., Mei, Q., Nie, J., Fu, X., and Han, W. (2015). Decitabine: a promising epimutagenic agent in solid tumors. *Expert Rev. Clin. Immunol.* 11, 363–375. <https://doi.org/10.1586/1744666X.2015.1002397>.
45. Tower, H., Ruppert, M., and Britt, K. (2019). The immune microenvironment of breast cancer progression. *Cancers* 11, 1375. <https://doi.org/10.3390/cancers11091375>.
46. Elhamamsy, A.R., Metge, B.J., Alsheikh, H.A., Shevde, L.A., and Samant, R.S. (2022). Ribosome biogenesis: a Central player in cancer metastasis and therapeutic resistance. *Cancer Res.* 82, 2344–2353. <https://doi.org/10.1158/0008-5472.CAN-21-4087>.
47. Vincenti, M.P., Coon, C.I., and Brinckerhoff, C.E. (1998). Nuclear factor kappaB/p50 activates an element in the distal matrix metalloproteinase 1 promoter in interleukin-1beta-stimulated synovial fibroblasts. *Arthritis Rheum.* 41, 1987–1994. <https://doi.org/10.1002/1529-0131>.
48. Borghaei, R.C., Rawlings, P.L., Jr., Javadi, M., and Woloshin, J. (2004). NF-kappaB binds to a polymorphic repressor element in the MMP-3 promoter. *Biochem. Biophys. Res. Commun.* 316, 182–188. <https://doi.org/10.1016/j.bbrc.2004.02.030>.
49. Farina, A.R., Tacconelli, A., Vacca, A., Maroder, M., Gulino, A., and Mackay, A.R. (1999). Transcriptional up-regulation of matrix metalloproteinase-9 expression during spontaneous epithelial to neuroblast phenotype conversion by SK-N-SH neuroblastoma cells, involved in enhanced invasivity, depends upon GT-box and nuclear factor kappaB elements. *Cell Growth Differ.* 10, 353–367.
50. Hiscott, J., Marois, J., Garoufalos, J., D'Addario, M., Roulston, A., Kwan, I., Pepin, N., Lacoste, J., Nguyen, H., Bensi, G., et al. (1993). Characterization of a functional NF-kappa B site in the human interleukin 1 beta promoter: evidence for a positive autoregulatory loop. *Mol. Cell Biol.* 13, 6231–6240.
51. Radisky, E.S., and Radisky, D.C. (2015). Matrix metalloproteinases as breast cancer drivers and therapeutic targets. *Front. Biosci.* 20, 1144–1163. <https://doi.org/10.2741/4364>.
52. Tulotta, C., and Ottewill, P. (2018). The role of IL-1B in breast cancer bone metastasis. *Endocr. Relat. Cancer* 25, R421–R434. <https://doi.org/10.1530/ERC-17-0309>.
53. Xu, C., Zhao, H., Chen, H., and Yao, Q. (2015). CXCR4 in breast cancer: oncogenic role and therapeutic targeting. *Drug Des. Devel. Ther.* 9, 4953–4964. <https://doi.org/10.2147/DDDT.S84932>.
54. Lin, K.T., and Wang, L.H. (2016). New dimension of glucocorticoids in cancer

- treatment. *Steroids* 111, 84–88. <https://doi.org/10.1016/j.steroids.2016.02.019>.
55. Scheinman, R.I., Gualberto, A., Jewell, C.M., Cidlowski, J.A., and Baldwin, A.S., Jr. (1995). Characterization of mechanisms involved in transrepression of NF-kappa B by activated glucocorticoid receptors. *Mol. Cell Biol.* 15, 943–953. <https://doi.org/10.1128/MCB.15.2.943>.
 56. Mikosz, C.A., Brickley, D.R., Sharkey, M.S., Moran, T.W., and Conzen, S.D. (2001). Glucocorticoid receptor-mediated protection from apoptosis is associated with induction of the serine/threonine survival kinase gene, sgk-1. *J. Biol. Chem.* 276, 16649–16654. <https://doi.org/10.1074/jbc.M010842200>.
 57. Wu, W., Chaudhuri, S., Brickley, D.R., Pang, D., Karrison, T., and Conzen, S.D. (2004). Microarray analysis reveals glucocorticoid-regulated survival genes that are associated with inhibition of apoptosis in breast epithelial cells. *Cancer Res.* 64, 1757–1764. <https://doi.org/10.1158/0008-5472.can-03-2546>.
 58. Pan, D., Kocherginsky, M., and Conzen, S.D. (2011). Activation of the glucocorticoid receptor is associated with poor prognosis in estrogen receptor-negative breast cancer. *Cancer Res.* 71, 6360–6370. <https://doi.org/10.1158/0008-5472.CAN-11-0362>.
 59. Setten, R.L., Rossi, J.J., and Han, S.P. (2019). The current state and future directions of RNAi-based therapeutics. *Nat. Rev. Drug Discov.* 18, 421–446. <https://doi.org/10.1038/s41573-019-0017-4>.
 60. Tsai, H.C., Li, H., Van Neste, L., Cai, Y., Robert, C., Rassool, F.V., Shin, J.J., Harbom, K.M., Beaty, R., Pappou, E., et al. (2012). Transient low doses of DNA-demethylating agents exert durable antitumor effects on hematological and epithelial tumor cells. *Cancer Cell* 21, 430–446. <https://doi.org/10.1016/j.ccr.2011.12.029>.
 61. Idrissou, M., Sanchez, A., Penault-Llorca, F., Bignon, Y.J., and Bernard-Gallon, D. (2020). Epi-drugs as triple-negative breast cancer treatment. *Epigenomics* 12, 725–742. <https://doi.org/10.2217/epi-2019-0312>.
 62. Yomtoubian, S., Lee, S.B., Verma, A., Izzo, F., Markowitz, G., Choi, H., Cerchietti, L., Vahdat, L., Brown, K.A., Andreopoulou, E., et al. (2020). Inhibition of EZH2 Catalytic activity Selectively targets a metastatic Subpopulation in triple-negative breast cancer. *Cell Rep.* 30, 755–770.e6. <https://doi.org/10.1016/j.celrep.2019.12.056>.
 63. Schneider, C.A., Rasband, W.S., and Eliceiri, K.W. (2012). NIH Image to ImageJ: 25 years of image analysis. *Nat. Methods* 9, 671–675.
 64. Varkonyi-Gasic, E., Wu, R., Wood, M., Walton, E.F., and Hellens, R.P. (2007). Protocol: a highly sensitive RT-PCR method for detection and quantification of microRNAs. *Plant Methods* 3, 12. <https://doi.org/10.1186/1746-4811-3-12>.
 65. Subramanian, A., Tamayo, P., Mootha, V.K., Mukherjee, S., Ebert, B.L., Gillette, M.A., Paulovich, A., Pomeroy, S.L., Golub, T.R., Lander, E.S., and Mesirov, J.P. (2005). Gene set enrichment analysis: a knowledge-based approach for interpreting genome-wide expression profiles. *Proc. Natl. Acad. Sci. USA* 102, 15545–15550. <https://doi.org/10.1073/pnas.0506580102>.
 66. Chiu, A.M., Mitra, M., Boymoushagian, L., and Collier, H.A. (2018). Integrative analysis of the inter-tumoral heterogeneity of triple-negative breast cancer. *Sci. Rep.* 8, 11807. <https://doi.org/10.1038/s41598-018-29992-5>.

STAR★METHODS

KEY RESOURCES TABLE

REAGENT or RESOURCE	SOURCE	IDENTIFIER
Antibodies		
Rap1B Rabbit Ab	CST	2326; RRID:AB_823626
CD44 Rabbit Ab	CST	37259; RRID:AB_2750879
IKK β Rabbit Ab	CST	8943; RRID:AB_11024092
β -actin Mouse mAb	Santa Cruz	sc-47778; RRID:AB_626632
mouse anti-rabbit IgG-HRP	Santa Cruz	sc-2357; RRID:AB_628497
goat anti-mouse IgG-HRP	Santa Cruz	sc-2005; RRID:AB_631736
Chemicals, peptides, and recombinant proteins		
Western Lightning Plus, Chemiluminescent Substrate	PerkinElmer	NEL105001EA
SuperSignal™ West Femto Maximum Sensitivity Substrate	Thermo Scientific	34095
TRIzol™ Reagent	Invitrogen	15596018
Chloroform Replacement Reagent (for Trizol)	Cyrusbioscience	CRSR
DMEM	Gibco	12100046
RPMI	Gibco	31800022
DMEM/F-12	Gibco	11330032
penicillin streptomycin	Gibco	30-002-CI
Horse serum	Gibco	26050070
EGF	Pro-Spec	CYT-217
Insulin	Sigma-Aldrich	I3536
hydrocortisone	Calbiochem	3867
cholera toxin	Sigma-Aldrich	C8052
Fetal Bovine Serum	HyClone	SH30396
Opti-MEM™ I Reduced Serum Medium	Gibco	31985070
TransIT-X2® Dynamic Delivery System	Mirus	MIR 6000
O-(Carboxymethyl)hydroxylamine hemihydrochloride	Sigma-Aldrich	C13408
Luciferase Assay Reagent	Promega	E1483
neolite Reporter Gene Assay System	PerkinElmer	6016716
Matrigel® Basement Membrane Matrix, Phenol Red-free, LDEV-free	Corning	356237
VivoGlo™ Luciferin, <i>In Vivo</i> Grade	Promega	P1043
Puromycin	Cyrusbioscience	101-58-58-2
Dexamethasone	Sigma-Aldrich	D4902
DAC (5-aza-2'-deoxycytidine)	Merck	A3656
TOPO TA cloning vector	Invitrogen	451641
Advantage 2 polymerase mix	Takara Bio Inc.	639201
8.0- μ m Falcon Cell Culture Inserts	Corning	353097
Corning® BioCoat® Matrigel® Invasion Chambers	Corning	354480
Critical commercial assays		
ReverTra Ace Set	PURIGO	PU-TRT-100
KAPA SYBR® FAST	Roche	KK4600
KAPA Probe® FAST	Roche	KK4701
UPL probe #21	Roche	N/A

(Continued on next page)

Continued

REAGENT or RESOURCE	SOURCE	IDENTIFIER
CellTiter 96® AQueous One Solution Cell Proliferation Assay (MTS)	Promega	G3580
EpiTect Bisulfite kit	Qiagen	59104
QIAamp genomic DNA kits	Qiagen	51304
RNeasy Mini Kit	Qiagen	74104
Deposited data		
RNA-seq data	GEO	GSE175867
Experimental models: Cell lines		
Human: MDA-MB-231	ATCC	CRL-12532
Human: HCC-1395	ATCC	CRL-2324
Human: Hs578T	ATCC	CRL-7849
Human: MCF-10A	ATCC	CRL-10317
Human: MCF-7	ATCC	HTB-22
Human: MDA-MB-231-GFP-luc-2A	This paper	N/A
Experimental models: Organisms/strains		
Mouse: C.B17/lcr-Prkdc ^{scid} /CrINarl	NARLabs	N/A
Oligonucleotides		
microRNA-708 precursor	Applied Biosystems	AM17100
microRNA-708-5p inhibitor	GeneDireX	N/A
Primers (Sequences are listed in Table S1)	Genomics	N/A
Recombinant DNA		
Plasmid: 4X NF-κB-responsive firefly luciferase reporter plasmid	Dr. Li-Chung Hsu from National Taiwan University.	N/A
Software and algorithms		
qPCRsoft version 3.4	Analytik Jena	N/A
<i>in vivo</i> imaging system (IVIS)	PerkinElmer	N/A
ImageJ	Schneider et al., 2012 ⁶³	N/A
Prism GraphPad	GraphPad Software	N/A
R	The R Foundation	N/A
RStudio	Posit	N/A
	The Cancer Genome Atlas (TCGA-BRCA)	https://portal.gdc.cancer.gov/projects/TCGA-BRCA
	Kaplan-Meier plotter Pan-cancer RNA-seq	https://kmplot.com/analysis/index.php?p=service&cancer=pancancer_maseq
	Wanderer	http://maplab.imppc.org/wanderer/
RNAseq data	This paper	GSE175867
R code used for analysis	This paper	https://doi.org/10.5281/zenodo.7779901

RESOURCE AVAILABILITY

Lead contact

Further information and requests for resources and reagents should be directed to and will be fulfilled by the lead contact, Kai-Ti Lin (ktlin@life.nthu.edu.tw).

Materials availability

This study did not generate new unique reagents.

Data and code availability

1. RNA-seq data have been deposited at GEO and are publicly available as of the date of publication. The accession number is GSE175867
2. Any additional information required to reanalyze the data reported in this paper is available from the [lead contact](#) upon request.
3. This paper does not generate the original code. R codes used for analyzing drug-drug interactions have been deposited at GitHub. DOI is listed in the [key resources table](#).

EXPERIMENTAL MODEL AND SUBJECT DETAILS

Animals

All animal procedures were performed in the National Health and Research Institutes (Miaoli, Taiwan) or National Tsing Hua University (Hsinchu, Taiwan) under the approved protocol by the Institutional Animal Care and Use Committee of National Health and Research Institutes (NHRI-IACUC-105053-AP) and National Tsing Hua University (NTHU-IACUC-109-011A). Eight-week-old female CB17/lcr-Prkdc scid/Crl mice were purchased from National Laboratory Animal Center (NLAC, Taiwan), and housed under standard laboratory conditions (temperature 24°C +/- 2°C, humidity 55% +/- 10%) in a 12 h light/dark cycle. The animal facility personnel monitored the animals daily, checking for levels of food and water in each cage. Mice were also physically checked three times a week by the researcher. The basic animal maintenance includes housing the mice in cages (four per cage), sufficient diet, water, and bedding. The cages were cleaned and sanitized on regular basis.

Human samples

Frozen breast tumor samples, adjacent nontumor tissues, and metastatic lymph nodes were obtained from the Department of Surgery, National Taiwan University Hospital (NTUH), under an approved IRB protocol (201605041RINA). Samples were collected during debulking surgery, and the identities of the patients remained anonymous. For data retrieved from The Cancer Genome Atlas (TCGA) database (<http://cancergenome.nih.gov/>), which is openly acquired from TCGA databases, ethics approval was not obtained and the need for informed consent was waived.

Cell lines

MDA-MB-231 (ATCC Cat# CRL-12532), HCC-1395 (ATCC Cat# CRL-2324), Hs578T (ATCC Cat# CRL-7849), and MCF-7 (ATCC Cat# HTB-22) cells were purchased from Bioresource Collection and Research Center (BCRC), Taiwan. MDA-MB-231, Hs578T, and MCF-7 cells were maintained in DMEM (Invitrogen, CA, USA) while HCC-1395 cells were maintained in RPMI (Invitrogen, CA, USA) containing 10% fetal bovine serum (FBS; HyClone, UT, USA) and 1 × penicillin-streptomycin (Invitrogen, CA, USA) at 37°C in an atmosphere containing 5% CO₂. Non-tumorigenic mammary epithelial line MCF-10A (ATCC Cat# CRL-10317) was cultured in DMEM/F-12 medium (Invitrogen, CA, USA) supplemented with 5% of horse serum (Invitrogen, CA, USA), 20 ng/mL of EGF (Pro-Spec, Rehovot, Israel), 10 µg/mL of insulin (Sigma-Aldrich, MI, USA), 0.5 µg/mL of hydrocortisone (Calbiochem, Darmstadt, Germany), 100 ng/mL of cholera toxin (Sigma-Aldrich, MI, USA), and 1% of 1 × penicillin-streptomycin (Invitrogen, CA, USA) at 37°C in an atmosphere containing 5% CO₂.

METHOD DETAILS

Transfection

Cells were transfected using TransIT-X2 (Mirus Bio, WI, USA) or RNAiMax (Invitrogen). The precursor miR-708 was from Applied Biosystems (Carlsbad, CA), and anti-miR-708 was from GeneDireX (Vegas, NV). MDA-MB-231 cell lines stably expressing GFP-luciferase were generated by infection with lentiviral particles encoding GFP-luciferase genes and then selected from the mass culture with puromycin (Sigma-Aldrich, MI, USA).

Nucleotides and reagents

All primer sequences are listed in [Table S1](#). Dexamethasone was purchased from Sigma-Aldrich (MI, USA). DAC (5-aza-2'-deoxycytidine) was obtained from Merck (Darmstadt, Germany). Antibodies against Rap1B (Cell Signaling, Cat# 2326), CD44 (Cell Signaling, Cat# 37259), and IKKβ (Cell Signaling, Cat# 8943), were

purchased from Cell Signaling Technology (MA, USA). The anti- β -actin antibody (SCBT, Cat# sc-47778) was obtained from Santa Cruz Biotechnology (CA, USA). The 4X NF- κ B-responsive firefly luciferase reporter plasmid is a kind gift from Dr. Li-Chung Hsu.

Quantitative real-time PCR analysis of mRNAs and miRNAs

RNA was extracted from cells using TRIzol (Invitrogen, CA, USA) following protocols supplied by the manufacturer. First-strand cDNAs were generated with ReverTra Ace (Toyobo, Japan) using oligo-dT primers or corresponding primers for specific miRNAs. Real-time RT-PCR was performed on a qTower 3 real-time PCR Thermal Cycler (Analytik Jena, Jena, Germany). The KAPA PROBE FAST universal qPCR Kit (KAPA Biosystems, MA, USA) together with Universal Probe Library #21 (Roche Applied Science, Penzberg, Germany) were used for miRNA detection,⁶⁴ while The KAPA SYBR FAST Universal qPCR Kit (KAPA Biosystems, MA, USA) was used for mRNA detection. The miRNA levels were normalized to U6 and mRNA levels were normalized to actin. Experiments were repeated 3 times. Data are presented as the normalized means \pm SD from three biological replicates.

Western blot analysis

Cells were lysed in 10 mM Tris buffer, pH 7.4, containing 0.15 M NaCl, 1% Triton X-100, 1 mM EDTA, and a protease inhibitor mixture (Roche, Basel, Switzerland). The cell lysates were resolved on SDS-polyacrylamide gel, transferred onto polyvinylidene difluoride (PVDF) membranes, and probed with antibodies. Experiments were repeated at least 3 times. Histograms present the normalized protein level with actin \pm SEM from three biological replicates. The uncropped Western blot images are shown in [Figure S7](#).

Transwell cell migration and cell invasion assays

Cell migration and invasion assays were performed in Boyden chambers as previously described.²⁷ Cell migration was assayed in 8.0- μ m Falcon Cell Culture Inserts (Corning, NY, USA), and the BD biocoat Matrigel invasion chamber (Corning, NY, USA) was applied for the cell invasion assay. Briefly, MDA-MB-231 cells ($0.5-1 \times 10^5$) or HCC-1395 cells (2×10^4) transfected with microRNA-708 (20 nM) or anti-microRNA-708 (50 nM) were pretreated with DEX (100 nM), DAC (1 μ M), or DEX+DAC in medium supplemented with 10% FBS for 48 h, and then suspended in DMEM with 1% FBS (500 μ L), and placed in the upper transwell chamber with a 0.3 cm² area. The bottom well was filled with 500 μ L of DMEM supplemented with 10% FBS and DEX, DAC, or together, as indicated above. After incubation for 18 h (migration) or 24 h (invasion), cells on the upper side of the inserts were removed with cotton swabs, and cells on the underside were fixed and stained with crystal violet. Photos of three regions were captured, and the number of cells was counted using ImageJ software (ImageJ, NIH). All experiments were repeated 3 times. Data are presented as the normalized means \pm SD from three biological replicates.

Cell proliferation assay

The cell proliferation assay was performed with CellTiter 96 Aqueous One Solution (Promega, WI, USA). The assay was performed according to the methods described in the manufacturer's manual. Briefly, cells ($1-3 \times 10^3$ cells) transfected with microRNA-708 (20 nM) or anti-microRNA-708 (50 nM) were seeded in 96-well plates and incubated with DEX (100 nM), DAC (1 μ M), or DEX+DAC for various times. At defined time points, 20 μ L of CellTiter 96 Aqueous One Solution Reagent were added and incubated with the cells for 2 h at 37°C. The quantity of formazan product, which is directly proportional to the number of living cells in the culture, was measured by recording the absorbance at 490 nm with a 96-well plate reader. All experiments were repeated three times. Data are presented as the means \pm SD from three biological replicates.

Bisulfite sequencing

Genomic DNA was extracted from MCF-10A or MDA-MB-231 cells using QIAamp genomic DNA kits (Qiagen, Hilden, Germany). The genomic DNA was treated with sodium bisulfite using the EpiTect Bisulfite kit (Qiagen, Hilden, Germany) according to methods described in the manufacturer's manual. The bisulfite-treated genomic DNA was then applied to PCR using the Advantage 2 polymerase mix (Takara Bio Inc., Japan). The PCR products were cloned into a TOPO TA cloning vector (Invitrogen, CA, USA), and ten individual clones from MCF-10A or MDA-MB-231 samples were sequenced. The percentage of methylation at each individual CpG island was calculated based on the bisulfite conversion results from the ten clones.

In vivo xenograft mouse model

MDA-MB-231 cells (2×10^6) with GFP-luciferase labeling were harvested and resuspended in 100 μ L of PBS containing 50% Matrigel (BD Biosciences, CA, USA). Cells were injected into the fourth mammary fat pad of 8-week-old female CB17/lcr-Prkdc scid/Crl mice. In the experiments with DEX and DAC treatment, 5 mg/mL of DEX was dissolved in ethanol and diluted in PBS for injection at a dose of 5 μ g/kg/time. DAC (100 mM) was dissolved in DMSO and further diluted in PBS for injection at a dose of 50 μ g/kg/time. DEX, DAC, or combined regimens were intraperitoneally injected into mice 3 times a week starting from day 5 after cell implantation. Tumor growth and abdominal metastases were monitored using live animal BLI (Caliper IVIS system, PerkinElmer, MA, USA) 40–60 days after implantation. Mice were intraperitoneally injected with luciferin and sacrificed 10 min later. Individual abdominal organ metastases were quantified from the ex vivo BLI signals of each organ.

RNA-seq analysis

MDA-MB-231 cells were treated with DMSO, 10 μ M DAC, 1 μ M DEX, or DAC+DEX for 6 days. RNA was extracted from cells using TRIzol (Invitrogen, CA, USA), cleaned up using the RNeasy Mini Kit (Qiagen, Hilden, Germany), and subjected to RNA-seq analysis (BIOTOOLS, Taiwan). Data obtained from high-throughput sequencing (Illumina NovaSeq 6000 platform) were transformed into raw sequenced reads by CASAVA base calling and stored in FASTQ format. FastQC (FastQC) and MultiQC (MultiQC) were used to check FASTQ files for quality. The obtained raw paired-end reads were filtered by Trimmomatic (v0.38) to discard low-quality reads, trim adapter sequences, and eliminate low-quality bases. The obtained high-quality data (clean reads) were used for subsequent analysis. Read pairs from each sample were aligned to the reference human genome GRCh38. "Relative Log Expression" normalization (RLE) was performed using DESeq2 (v1.22.1) with biological triplicates. Differentially expressed genes (DEGs) in two conditions were analyzed with R using DESeq2 (with biological triplicates). Detailed information is provided in [Data S1](#). The gene set enrichment analysis (GSEA)⁶⁵ was performed to identify enriched biological functions and activated pathways from the molecular signature database (MSigDB). The accession number for the RNA sequencing data produced in this study is GEO: GSE175867. The interaction between DAC and DEX was determined with the "lm" function in R. Briefly, a model matrix was constructed based on a multiple linear regression equation: "Y ~ DAC + DEX + DAC: DEX". The strength and significance of the interaction for each gene are the coefficient and p value of the interaction term "DAC: DEX".

Kaplan–Meier plotter database analysis

Kaplan–Meier Plotter (<http://kmplot.com/analysis/>) is an online database of published microRNA array datasets that assesses the effect of 54,675 genes on survival using 2,339 breast cancer samples from different databases, including the METABRIC database (n = 1262) and TCGA database (n = 1077). We performed a Kaplan–Meier Plotter analysis to assess the prognostic value of miR-708 in patients with the pan breast cancer or TNBC subtype. The hazard ratios (HRs) with 95% confidence intervals (CIs) and log rank p values were also computed.

Retrieving miRNA-seq and methylation array data from The Cancer Genome Atlas

The normalized miRNA-seq data containing 989 breast cancer (BRCA) cases, 163 breast normal tissues, and patients' clinical information were retrieved from TCGA. Patients (n = 164) were identified as having TNBC based on the analysis performed by Chiu et al.⁶⁶ Detailed clinical information is provided in [Table S4](#). Wanderer,³⁹ a web analytics platform designed to assess and visualize gene expression and DNA methylation profiles from TCGA, was applied to reveal the position of the CpG sites on the chromosome analyzed with the methylation array and to analyze the methylation status of the CpG sites in the promoter region of miR-708. Seven hundred sixty-six patients with breast cancer (BRCA) were included to analyze the methylation level of the CpG sites at the promoter region of miR-708 and its correlation with patient survival. The detailed information is summarized in [Table S5](#). For the Kaplan–Meier survival analysis, we divided the beta values into low (0–0.25) and high (0.25–1) methylation levels at specific CpG probes, including cg11968091, cg14309111, cg15355859, cg19842216, and cg11862642, and performed a log rank test to assess the difference in survival between the two groups. The statistical significance was determined using the χ^2 test.

QUANTIFICATION AND STATISTICAL ANALYSIS

The statistical analyses were all performed using GraphPad Prism software (GraphPad Prism, CA, USA) with Student's t test to compare two means. ANOVA followed by Tukey's post hoc test was used for the statistical analysis when more than two means were compared (*p < 0.05; **p < 0.01; ***p < 0.001; ****p < 0.0001).